



저작자표시-비영리-변경금지 2.0 대한민국

이용자는 아래의 조건을 따르는 경우에 한하여 자유롭게

- 이 저작물을 복제, 배포, 전송, 전시, 공연 및 방송할 수 있습니다.

다음과 같은 조건을 따라야 합니다:



저작자표시. 귀하는 원저작자를 표시하여야 합니다.



비영리. 귀하는 이 저작물을 영리 목적으로 이용할 수 없습니다.



변경금지. 귀하는 이 저작물을 개작, 변형 또는 가공할 수 없습니다.

- 귀하는, 이 저작물의 재이용이나 배포의 경우, 이 저작물에 적용된 이용허락조건을 명확하게 나타내어야 합니다.
- 저작권자로부터 별도의 허가를 받으면 이러한 조건들은 적용되지 않습니다.

저작권법에 따른 이용자의 권리는 위의 내용에 의하여 영향을 받지 않습니다.

이것은 [이용허락규약\(Legal Code\)](#)을 이해하기 쉽게 요약한 것입니다.

[Disclaimer](#)

공학석사 학위논문

파우더 베드 퓨전 방식의 적층 제조
시뮬레이션을 이용한 마레이징강 C300
분말소재의 스케일링 계수 보정에 관한 연구

**A Study on Calibration for Scaling Factor of Maraging Steel
C300 Powder Material by Using Additive Manufacturing
Simulation of the Powder Bed Fusion Method**

울산대학교 대학원
기계자동차공학과
장고기

파우더 베드 퓨전 방식의 적층 제조
시뮬레이션을 이용한 마레이징강 C300
분말소재의 스케일링 계수 보정에 관한 연구

지도교수 염영진

이 논문을 공학석사 학위 논문으로 제출함

2021년 02월

울산대학교 대학원
기계자동차공학과
장고기

**A Study on Calibration for Scaling Factor of Maraging Steel
C300 Powder Material by Using Additive Manufacturing
Simulation of the Powder Bed Fusion Method**

Supervisor : Professor Young Jin Yum

**Submitted to the Office of Graduate School of
University of Ulsan**

In partial Fulfillment of the Requirements for the Degree of

Master of Science

By

GAOQI ZHANG

Department of Mechanical Engineering

University of Ulsan

Ulsan, Republic of Korea

February 2021

장고기의 공학 석사학위 논문을 인준함

심사위원 천 두 만



심사위원 주 석 재



심사위원 염 영 진



울산대학교 대학원

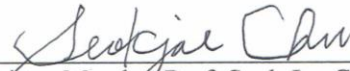
2021년 02월

**A Study on Calibration for Scaling Factor of Maraging Steel C300 Powder
Material by Using Additive Manufacturing Simulation of the Powder Bed
Fusion Method**

This certifies that the master's thesis of GAOQI ZHANG is approved by



Committee Chair Prof. Doo Man Chun



Committee Member Prof. Seok Jae Chu



Committee Member Prof. Young Jin Yum

ACKNOWLEDGEMENTS

The completion of the thesis is attributed to many peoples support and encouragement.

Sincerely, I am very grateful to my professors for guidance, Prof. Young Jin Yum Prof. Yong Seok Kim Prof. Soon Yong Yang. Their conscientious academic spirit and modest, open-minded personality inspire me both in academic study and daily life.

Second, I am honored to meet the brothers in our laboratory.

Last but not least, I would like to express my special thanks to my parents whose care and support motivate me to move on and make me want to be a better man.

ABSTRACT

This study was conducted with the aim of establishing a simulation method that corrects the scaling factor in order to improve the accuracy of the simulation software in the additive manufacturing process of Maraging Steel C300 powder material. For this study, two studies were conducted to achieve the aims. First, the shape of the Additive Manufacturing sample was analyzed through literature investigation on the existing Additive Manufacturing simulation research. And the sample shape for Additive Manufacturing simulation of this study was selected from the analyzed result. Second, based on the selected sample shape, the scaling factor was corrected through the manufacture and measurement of Additive Manufacturing samples and iterative simulation. The procedure for calibration of the scaling factor was performed through the manufacture of an AM sample, measurement of deformed distortion and iterative simulation, based on the selected cantilever beam shape. For the manufacture of the Additive Manufacturing sample, the C300 powder material of Maraging Steel and Powder Bed Fusion method equipment were used. The distortion measurement of the manufactured Additive Manufacturing sample was performed before and after removal of the support according to the simulation purpose. The parameters for powder materials and equipment required for sample manufacture were applied from the optimized environment provided by the manufacturer. All parameters for the powder material and equipment used to prepare the Additive Manufacturing sample were applied equally to the scaling factor simulation. Simulations for scaling factor correction were performed for Assumed Strain mode, Thermal Strain mode and Pattern Scanning mode respectively. In addition, the Pattern Scanning mode simulation was

performed for the scanning (starting and rotating) angles of 0° , 90° and 67° respectively. Distortion was measured from each simulation result and the scaling factors SSF and ASC were calculated. These simulation and calculation process were repeated until the distortion error was less than 1%. The scaling factors SSF and ACS for the cantilever beam in this study are as follows: First, the correction value SSF of the optimized shape in the assumed strain and scanning mode is 15.89, while in the thermal strain mode, the SSF is optimized value is 8.3892. (at point A) Second, the correction value ASC_{\parallel} and ASC_{\perp} of the optimized shape in the scanning mode is both 1, and the value of $ASC_{\parallel} = 1.0048, ASC_{\perp} = 0.9952$ in the thermal strain mode respectively. (at point A) Third, the correction value SSF of the optimized shape in the assumed strain mode is 33.41 scan pattern mode is 31.65, while in the thermal strain mode, the SSF is optimized value is 17.3105. (at point B) Forth, the correction value ASC_{\parallel} and ASC_{\perp} of the optimized shape in the scan pattern simulation is $ASC_{\parallel} = 0.29, ASC_{\perp} = 0.71$, and the value of $ASC_{\parallel} = 0.2962, ASC_{\perp} = 1.7038$ in the thermal strain simulation respectively (at point B).

The final validation of the scaling factor derived through this study can be confirmed through shape compensation of the AM sample and manufacturing of the AM sample. However, it was not verified in this study. Therefore, this study needs additional research in the future.

Keywords: Additive Manufacturing (AM) Simulation, Scaling Factor, Strain Scale Factor (SSF), Anisotropic Strain Factor (ASC), Metal 3D Printing, Powder Bed Fusion (PBF), Maraging Steel C300

CONTENTS

CONTENTS	i
List of Figures	iii
List of Tables.....	v
Chapter 1 Introduction.....	1
1.1 Challenges and problems in development.....	2
1.2 Investigation and analysis of existing research	3
1.3 Research method	6
Chapter 2 Background.....	10
2.1 Metal 3D Printing AM Technology and Machine.....	10
2.2 Maraging Steel C300	13
2.3 AM Simulation Process of ANSYS	17
2.4 Extracting Distortion Data	21
2.5 Scaling Factor Calculation	22
Chapter 3 AM Simulation Geometry Review.....	27
Chapter 4 Experiment.....	36
4.1 AM Sample Geometry	36
4.2 AM Sample Manufacture.....	36
4.3 Taking Distortion Measurements.....	41
4.4 Simulation approach	43
Chapter 5 Results and discussion	47
5.1 Calibration of SSF and ASCs for the measurement Point A.....	47
5.2 Fine calibration of SSF and ASCs for the measurement Point A.....	51

5.3 Calibration of SSF and ASCs for the measurement Point B	54
5.4 Fine calibration of SSF and ASCs for the measurement Point B.....	57
Chapter 6 Conclusion	61
6.1 Research results	61
6.2 Future research topics	65
REFERENCE	66

List of Figures

Fig. 1 Research process.....	8
Fig. 2 Powder size distribution and morphology (SEM)	16
Fig. 3 AM process simulation flow chart with ANSYS Additive Suite [39]	18
Fig. 4 AM process simulation processor using ANSYS Additive Suite.....	19
Fig. 5 AM simulation processor using Additive Print	20
Fig. 6 Schematic of the point coordinates for the distortion measurement	22
Fig. 7 Schematic of the distortion data extraction method	22
Fig. 8 Process flow for the SSF and ASCs calculations [38].....	23
Fig. 9 Maximum distortion according to AM shape and AM simulation mode.....	35
Fig. 10 Cantilever beam dimensions [38]	36
Fig. 11 Cantilever beam with support[38]	36
Fig. 12 Layout of AM sample for the additive manufacturing	37
Fig. 13 Scan pattern (a) (0°, 0°) [38]	38
Fig. 14 Scan pattern (b) (90°, 0°) [38]	39
Fig. 15 Scan pattern (c) (rotating stripe) [38]	39
Fig. 16 AM Sample before wire cutting	40
Fig. 17 AM Sample after wire cutting	41
Fig. 18 Simulation setup screen for scaling factor correction	45
Fig. 19 Extract data from AM simulation outputs	46
Fig. 20 Distortion of Assumed Strain simulation	48
Fig. 21 Distortion of Scan Pattern simulation.....	49
Fig. 22 Distortion of Thermal Strain simulation.....	50
Fig. 23 Fine tuning distortion of Assumed Strain simulations	52

Fig. 24 Fine tuning distortion of Scan Pattern simulation	53
Fig. 25 Fine tuning distortion of Thermal Strain simulation	53
Fig. 26 Distortion of Assumed Strain simulations.....	55
Fig. 27 Distortion of Scan Pattern simulation.....	56
Fig. 28 Distortion of Thermal Strain simulation.....	57
Fig. 29 Fine tuning distortion of Assumed Strain simulations	58
Fig. 30 Fine tuning distortion of Scan Pattern simulation	59
Fig. 31 Fine tuning distortion of Thermal Strain simulation	60

List of Tables

Table 1 AM method classification of material type, power source type, and according to laser manufacturer.....	12
Table 2 Chemical composition of c300 powder	16
Table 3 Material parameters for the AM simulation of C300 powder	17
Table 4 Spreadsheet for calculating scaling factors (case of Scan Pattern) [38].....	24
Table 5 Variable & Subscripts of spread sheet.....	24
Table 6 Review of AM simulation sample shape in existing research	28
Table 7 Simulation result according to AM sample geometry	31
Table 8 AM simulation result according to AM shape and simulation mode	34
Table 9 Build-up parameters.....	40
Table 10 Distortion measurement of AM sample by vernier calipers	42
Table 11 Distortion measurement of AM sample by 3D scanning.....	42
Table 12 3D scan sample measurement results of point A and B	43
Table 13 Calibration of SSF by Assumed Strain simulation	48
Table 14 Calibration of SSF and ASCs for Scan Pattern simulation.....	48
Table 15 Calibration of SSF and ASCs for Thermal Strain simulation.....	50
Table 16 Calibration of SSF for Assumed Strain simulations.....	52
Table 17 Calibration of SSF and ASCs for Scan Pattern simulation.....	52
Table 18 Calibration of SSF and ASCs for Thermal Strain simulation.....	53
Table 19 Calibration of SSF Assumed Strain simulations	55
Table 20 Calibration of SSF and ASCs for Scan Pattern simulation.....	56
Table 21 Calibration of SSF and ASCs for Thermal Strain simulation.....	57
Table 22 Calibration of SSF Assumed Strain simulations	58

Table 23 Calibration of SSF and ASCs for Scan Pattern simulation.....	59
Table 24 Calibration of SSF and ASCs for Thermal Strain simulation.....	60

Chapter 1 Introduction

Additive Manufacturing (AM) is very useful for realizing advanced customization because it can be easily controlled to be implemented in a special feature or with different materials based on the basic design once designed. The ability to produce highly customized products at once can significantly reduce production costs and material waste, while significantly improving user satisfaction and corporate profits.

In particular, the application of additive manufacturing technology in the development stage of metal products has been known to have great strategic and financial effects. However, it is not generalized to all companies and is mainly applied to large corporations such as airline companies that require high-cost and sophisticated product design. This is known to be because the printing equipment used for metal additive manufacturing is expensive, the cost of the material powder is remarkably high, and the failure rate is high in the early stage of technology, resulting in a large initial cost of building a development environment. Stefaan Motte (Materialize.Inc.) said that over 75% of the total cost of additive manufacturing using metal 3D printing goes into the printing process. It is also said that a lot of costs are incurred for test printing or failed printing. Especially, it is said that an average of 15% of printed outputs with complex geometric structures fail [1]. Siemens' Eckhoff said it would take an average of three to five attempts to complete the current metal printing job. And, said that as more and more companies and industries gradually adopt additive manufacturing as part of their production workflows, achieving the finished output at once is becoming more and more important [2]. In metal printing, the failure to produce finished prints at

once and repeated trial and error is due to the following factors in the introduction of new equipment or workflows. There may be a lack of accumulated technology, adjustment of unfamiliar manufacturing parameters, manufacturing errors resulting from lack of experience, and factors due to insufficient removal of unnecessary elements, etc. Trial-and-error failure can be reduced by minimizing or optimizing the aforementioned factors, and this can be mostly solved through the predictive simulation by software.

Recently, simulation studies have been actively conducted in the AM field of metal 3D printing in consideration of the function of the final product as in the traditional MC processing field. Failure rate of the additive manufacturing can be reduced by predicting and correcting problems that may occur in the pre-processing , the additive process, and the post-processing process in the AM process of metal 3D printing.

1.1 Challenges and problems in development

Today, 3D printing service is operating in an increasingly cost-competitive environment and are constantly looking for ways to increase productivity and efficiency. In a typical process of CAD to printed part, the actual printing, including machine and material costs, accounts for more than 75 percent of the total cost. As a result, running multiple test prints and printing failed or unsuitable parts is very costly. This is especially the case for metal 3D printing and the production of high-value, customizable metal components with complex geometries. On average 15 percent of these metal parts fail.

In the metal additive manufacturing process, the substrate and the cladding layer

are prone to defects such as deformation, pores and poor fusion, and the solidification microstructure in the molten pool is also affected by process parameters. To obtain components with high forming accuracy, no internal defects, and excellent solidification microstructure control, it is necessary to conduct in-depth research on the thermal process of metal additive manufacturing and the internal transmission of the molten pool and the solidification microstructure. The complex interaction of laser, molten pool and powder in the metal additive manufacturing process makes it very difficult to use experimental analysis methods to accurately reveal the metal additive manufacturing process.

Residual stress caused by this unique thermal cycle in metal AM is a critical issue for the manufactured parts since the steep residual stress gradients would generate part distortion. A during process part distortion may result in scraper blade damage in the case of Powder Bed Fusion, distortion of the final part would dramatically deteriorate its functionality.

1.2 Investigation and analysis of existing research

The use of computer simulation methods has become a study on the metallurgical and solidification behavior of metal additive manufacturing. With simulation, operators can predict and analyze the behavior of a part during physical production by creating a virtual prototype, helping optimize their build preparation and reduce the number of costly reprints and fails. And now there are many studies on the simulation of residual stress and deformation in order to enable the simulation results to be put into practical work. Distribution and evolution of residual stress in metal parts are very complicated.

Kruth et al. [3] conducted research on residual stress in metal additive manufacturing earlier. Research shows : (a) the residual stress along the laser scanning direction is much larger than the vertical scanning direction; (b) the residual stress presents a "tension-compression-tension" distribution from top to bottom; (c) the height of the workpiece, the thickness of the substrate, Heat treatment etc. have a great influence on the residual stress.

Bass et al. [4] used SLM to form hollow and solid cylindrical Ni-based 625 alloys, and used neutron diffraction to measure the axial, radial and circumferential residual stresses at different heights. The results show that: (a) the axial and circumferential residual stresses are tensile stresses on the outer surface and compressive stresses on the inside; (b) the axial residual stress values are the largest, while the radial residual stress values are the smallest; (c) in the comparison of different heights, the axial and circumferential residual stress values of the upper surface of the formed part are the smallest; (d) the residual stress value of the hollow cylinder is smaller than that of the solid cylinder.

Hodge et al. [5] of Lawrence Livermore National Laboratory used thermal finite element simulation to calculate the evolution of the residual stress of the L-shaped structure and found that the residual stress has a "tension-compression-tension" change trend along the depth direction. Especially the increase after the material manufacturing part is separated from the substrate, the residual compressive stress becomes more obvious. For L-shaped members, the residual tensile stress levels around the corners are significantly higher.

Su Rez et al. [6] laser cladding Co-based alloy satellite 6B on the surface of 304 stainless steel, and used the energy scattering XRD method to measure the residual stress distribution along the height, which also showed "tension-compression-tension" The distribution characteristics.

Brown et al. [7] used neutron diffraction to more completely show the changes in the three-dimensional residual stress of the SLM in the plane and height. The results showed that the stress distribution in the same plane was basically the same, but there were obvious changes along the height direction. It is the residual stress along the scanning direction that changes from tensile stress to compressive stress from top to bottom. In addition, the residual tensile stress value along the scanning direction is larger than other directions.

Moat et al. [8] used the profile method to measure the residual stress distribution along the height direction, and verified the measurement results of the profile method with the neutron diffraction method. The results showed that the stress along the scanning direction gradually changed from tensile stress to compressive stress, and finally to tensile stress, while the residual stress along the height direction gradually evolved from slight tensile stress to compressive stress.

Ding et al. [9] used neutron diffraction and finite element simulation to obtain the evolution of residual stress in the arc additive manufacturing layer 1, 2, and 3. With the increase of the accumulation layer, the residual stress on the upper surface along the scanning direction stress is slightly reduced, and the residual stress in other directions does not show a significant change.

Mukherjee et al. [10] used finite element simulation to compare the residual stress between 2 and 10 thin-walled stacks. It is obvious that as the number of stacked layers increases, the compressive stress area becomes larger and larger, and the largest appears at the “wall foot” residual tensile stress.

From the process analysis, Alessandro et al. [11] used the deep hole method to accurately measure the residual stress value of the selected area of laser melting AlSi10Mg along the upper surface to a depth of 1 mm, and found that the stress relief annealing can effectively reduce the residual stress level.

Bailey et al. [12] measured the residual stress of laser-melted-deposited H13 steel using the layer-stripping XRD method, and believed that a larger volume fraction of martensite caused the generation of compressive residual stress on the upper surface.

Szost et al. [13] compared the residual stress state of laser melting deposition and arc additive manufacturing parts, and found that the three-dimensional residual stress distribution law of the two processes is basically the same, and the maximum tensile stress value of arc additive parts is slightly higher than that of laser melting the deposited pieces.

1.3 Research method

Modeling the additive manufacturing process can not only provide important insights into the competitive physical phenomena that lead to the final material performance and product quality, but also lay the foundation for manufacturing process certification, thereby providing design space and materials for functional products. The theoretical model and numerical simulation of laser material processing are developing

simultaneously with the application of laser. In the early days of experimental research on laser fusion and laser cladding, people have begun extensive theoretical research and numerical simulation.

Whether it is selected area laser melting or laser three-dimensional forming, the manufactured parts usually have complex residual stresses. Among them, the tensile residual stress has an adverse effect on the performance of the parts, reducing the effective fatigue and tensile properties of the structure. In addition, the residual stress of the part can cause the part to deform, so that the shape of the part does not match the shape of the designed part. Computer simulation of the residual stress in the metal additive manufacturing process usually uses the finite element method to simulate the additive process in the form of finite element model elements.

The basic theoretical research on the formation and evolution process of residual stress and deformation in the metal laser additive manufacturing process has been gradually improved. In order to realize the control of stress and deformation in the laser additive process, the current research mainly focuses on the simulation and prediction analysis of laser additive stress and deformation. Based on this, it provides guidance for subsequent stress and deformation control. The finite element simulation calculation has huge advantages for the stress calculation in the laser additive manufacturing process, but when the size of the part is large, the finite element calculation faces the situation that the calculation amount is too large to meet the actual needs. The simulation efficiency and accuracy of stress deformation still need to be improved, and multi-scale simulation technology should be continuously improved to meet the

prediction of stress and deformation of large-scale laser additive structures.

In the research, we use the built-in AM module in ANSYS Additive Print software to study the macroscopic simulation of the process of AM components printed with C300. In the macro analysis of the manufacturing process, SSF and ASC are two important process parameters. By modifying the two process parameters, improve the accuracy of the finite element prediction model, which in turn affects the prediction of residual stress and deformation in the final result.

The verification process of the research content is realized through the following steps as shown in Fig. 1:

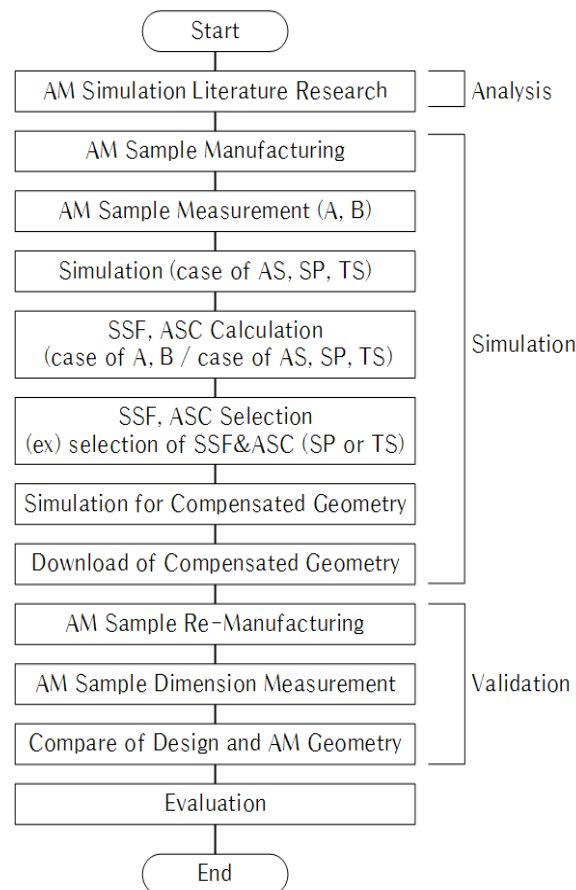


Fig. 1 Research process

In addition, the Strain Scaling Factor (SSF) is a calibration factor used to account for differences in machines that you may use to improve the accuracy of your

simulations. And Anisotropic Strain Coefficients (ASC) are used to represent anisotropic strain behavior on coordinate systems aligned with the local longitudinal, transverse, and depth scan directions. Positive values result in compressive base strain (contraction), whereas negative values result in tensile strain (expansion) [37].

The first step in simulation is the material condition of the Additive Manufacturing (AM) samples, setting the same machine parameters and materials, and measuring and recording the amount of distortion of the AM samples at positions A and B. Similarly, the inherent Strain mode, Scanning Strain mode and Thermal Strain mode are used to running the first simulation of the sample. Three simulation models are used to calculate SSF and ASC using information from different positions of A and B. In order to optimize ANSYS' SSF and ASC values, we need to choose the results between Scanning the Strain mode and Thermal Strain mode. This choice will have a great impact on the optimization results. After the system has optimized the SSF and ASC, it will use these optimized values to obtain a compensated shape. And, download the calibrated the .stl file from the simulator to get the compensated shape. At this point, the optimization process has been completed. Send the compensated shape to the manufacturer to rebuild and measure the AM sample to confirm the optimized SSF and ASCs values. By measuring the distortion of the secondary-manufactured AM sample, the design shape and the additive manufacturing shape are compared to observe the influence of residual stress and thermal stress on the amount of deformation of the additively manufactured sample. At this time, the evaluation of the optimized SSF and ASCs values is completed.

Chapter 2 Background

2.1 Metal 3D Printing AM Technology and Machine

3D printing technology is a layering method in which a 3D shape is converted into digital CAD model data through computer modeling, cut into two-dimensional planes, and then powdered materials are stacked on the plane by a three-dimensional printer. (by layer). While the conventional manufacturing technology was a subtractive manufacturing method that produces a three-dimensional object by cutting or shaving a three-dimensional material through machining, etc., in 3D printing, the method of stacking in a concept that is contrary to this is adopted. It is used in additive manufacturing (AM) or rapid prototyping (RP). The field of additive manufacturing began with polymer materials and recently expanded to metal materials, and 3D printing technology is rapidly developing. According to a report by Global Financial Group ING, by 2060, 50% of manufactured products will be printed on 3D printers, accounting for more than a quarter of the world's trade volume. Interest in the metal 3D printing AM field is expected to increase day by day. However, in the 3D printing AM process, there are a number of problems that must be solved first. Prototype production at the stage of developing a product with a complex shape has advantages in terms of cost and time, but at the level of the production stage, slow speed, low precision, low strength, and material limitations are the first to be solved.

ASTM (American Society for Testing and Materials) and ISO (International Organization for Standardization) for metal 3D printing techniques are largely classified into two categories. It consists of a powder bed fusion (PBF) method in which a flatly laid powder area is fused with the selective thermal energy of a laser, and a

high-energy direct irradiation method (Directed Energy Deposition) in which a powder material is directly melted and deposited with the concentrated thermal energy of a laser beam. DED). As such, metal 3D printing techniques are largely divided into PBF and DED methods. They are further classified according to the type of material and type of power source, and are called by various names depending on the laser manufacturer. Table 1 shows the classification of the AM method according to the type of material, type of power source, and laser manufacturer.

The PBF method irradiates a laser beam to a two-dimensional cross section of a three-dimensional shape to be processed on the powder (plastic, ceramic, metal) flatly supplied by a powder supply device (called a squeegee, blade and etc.). After sintering, the process of supplying new powder on it is repeated several times to create a desired three-dimensional shape. In this process, the thickness of the laminated powder is about 30~150 μm . Most of the laser beams used as heat sources use CO₂ laser beams, and the size of the beam oscillated by the laser beam engine is about 500 μm . In the PBF method, the powder material mainly uses spherical powder in the range of 10 to 45 μm . In general, it is known that the shape of a powder material is better as it is closer to a spherical shape, and the layer ability is excellent as it has a composition of fine particles having a uniform size. However, if the powder particle size is too fine, micro-explosion may occur and the powder may be blown or carbonization may occur instead of sintering. As such, the selection of the size and shape of the powder particles is one of the major processes.

Table 1 AM method classification of material type, power source type, and according to laser manufacturer

	Material type	Power source	AM Process	
PBF	Powder based	Laser	SLS (Selective Laser Sintering)	
			DMLS (Direct Metal Laser Sintering)	
			SLM (Selective Laser Melting)	
		Electron beam	EBM (Electron Beam Melting)	
DED		Laser	Laser	LENS (Laser Engineered Net Shaping)
				DMD (Direct Metal Tooling)
				DMT (Direct Metal Tooling)
				CLAD (Construction Laser Additive Direct)
	Solid Filler based	Electron beam	EBAM (Electron Beam Additive Manufacturing)	
		GTSW, GMAW arc	WAAM (Wire Arc Additive Manufacturing)	
		GMAW arc	DML (Direct Metal Lamination)	
			ADED (Arc Directed Energy Deposition)	
		Plasma arc	IFF (Ion Fusion Formation)	
			RPD (Rapid Plasma Deposition)	
GTAW arc	STAM (Super-TIG Additive Manufacturing)			

The main process variables of the PBF method (example of W company equipment) include sample orientation (Horizontal/Vertical), building strategy (Island/Linear; Size-mm; Rotation-°), and laser power: W), hatch spacing (μm), scanning speed (mm/s), layer thickness: μm , energy density (j/mm^3), and the like. The PBF method has the advantage of being able to implement relatively high precision (compared to DED), expandability to various materials, and free design (complex) shape. In addition,

since the un-melted powder acts as a supporter, the simple shape also has the advantage that a separate supporter is not required. However, problems in the treatment of fume and dust generated inside the chamber during the lamination process (which affects the quality), the treatment and recycling of materials after lamination, and low durability of the laminated products are challenges to be solved. In addition, when the stacking shape is complex and the space is formed in a wide space, a supporter must be considered inevitably in order to stack a more precise product. Regarding the supporter, in the early days of additive manufacturing technology, it was analyzed that the influence on the supporter was insignificant compared to other process factors and has been ignored. Recently, the demand for the precision of products has increased, and the influence of structural deflection or thermal deformation on the precision of laminated products in the process of lamination has been verified, and has been considered important.

2.2 Maraging Steel C300

18Ni300 maraging steel is an ultra-high-strength steel with carbon-free or ultra-low-carbon Fe-Ni martensite as the matrix and aging treatment to make the intermetallic compound precipitation hard enabled. The strength of this type of steel does not come from carbon, but from the precipitation of intermetallic compounds. The alloying elements that play a role in age hardening in steel are titanium, aluminum, cobalt, and molybdenum. After aging treatment, the thermal deformation is small, the machining and welding performance is excellent, the heat treatment process is simple, and the size shrinkage is uniform and stable. Therefore, the 18Ni300 maraging steel

material has been widely used in the mold field. However, impurities have a great influence on the performance of maraging hardened steel, and the effect on steel with higher yield strength is more obvious.

Carbon-containing martensite is strengthened by austenite non-diffusion transformation into body-centered cubic metastable martensite. The main problem is the insufficient toughness of carbides, which makes the steel more brittle and limited in strength. When the maraging steel is heated to a high temperature, the alloying elements in the maraging steel are fully integrated into the single-phase austenite structure, and then the temperature is reduced to start martensite transformation, the lath martensite is a structure obtained at room temperature, then through aging treatment, the second phase intermetallic compound is precipitated in the supersaturated martensite to perform dispersion strengthening of the metal.

18Ni30 is mainly used for precision forging dies to make high-precision, super-mirror, complex cavity, large cross-section, mass production plastic molds. 18Ni300 mold steel powder can print the front and back mold cores, inserts, sliders, guide posts and hot runner water jackets of injection molds, which has the advantages of reducing molding cycle, improving product quality, and more uniform mold temperature field. Industrially, maraging steel is designed to provide specific levels of yield strength ranging from 1030-2420 MPa. Some experimental maraging steels have yield strengths as high as 3450 MPa.

The deformation of the mold after heat treatment is one of the three major problems of mold heat treatment (deformation, cracking, hardening). Pre-hardened plastic mold

steel solves the problem of mold heat treatment deformation, but the mold requires high hardness and causes difficulties in mold processing. Melting not only maintains the processing accuracy of the mold, but also makes the mold have higher hardness. For complex, precise, and long-life plastic molds, it is an important problem faced by mold materials. To this end, a series of age-hardening plastic mold steels have been developed. After quenching (solid solution), the mold parts become soft (hardness is about 28~34 HRC), which is convenient for cutting and forming, and then age hardening to obtain the required comprehensive mechanical properties.

2.2.1 C300 Powder Material

In this paper, gas (Argon) atomized and alloyed C300 powder of the maraging steel grade is used as the working material for the additive manufacturing (AM) samples. Fig. 2 (a) lists the diameter statistics of the powder particles used. The C300 powder has a wide diameter distribution from 0 to 150 μm . It can be seen that 50-70 μm occupies the highest proportion and the average powder size is around 60 μm . Fig 2 (b) highlights the particle shape and regularity of the powder materials used as observed using SEM. The two dissimilar particle shapes (irregular and spherical) are the result of the atomization process in the manufacturing process. It's chemical composition is presented in Table 2. In order to better perform the simulation analysis process and accurately its simulation results, systematically investigated the mechanical properties of C300 powder and applied it to the simulation process. The physical properties of the material powder differ depending on the source and literature. This means that material testing and interpretation must be performed together for accurate interpretation.

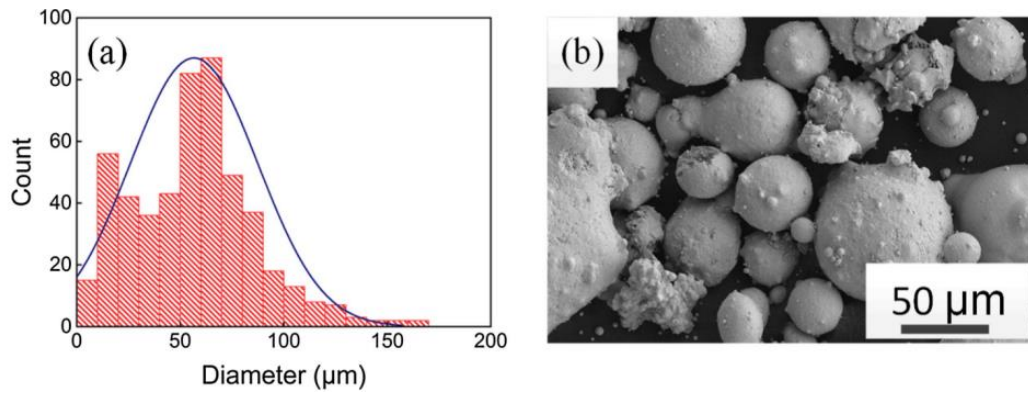


Fig. 2 Powder size distribution and morphology (SEM)

Table 2 Chemical composition of C300 powder

	Fe	Ni	Co	Mo	Ti	C	Mn	Cr
C300 [Ref]	Balance	17.0-19.0	8.0-10.0	4.5-5.5	0.8-1.2	< 0.03	<0.15	<0.25

2.2.2 Material parameters for the AM Simulation of C300 powder

The parameters for AM simulation of C300 powder are shown in Table 3. This has been referenced from existing literature, and environmental parameters of the manufacturer's machine. The parameters presented here are used equally for AM sample preparation.

The physical properties of the material powder differ depending on the source and literature. This means that material testing and interpretation must be performed together for accurate interpretation. By comparing the experimental value and theoretical value based on the sample, and then repeat the analysis for different target materials, so as to obtain the required powder mechanical property values [14]. Yan et al.[15] analyzed the microstructure and surface characteristics of four widely used steels (316L, H13, P20, and 18Ni300), and detailed the relationship between the microstructure of the powder and the laser absorption rate. XPS research results show

that all four steel powders have a layered surface structure, consisting of a thin layer of iron oxide on the outermost layer and a metal matrix on the inner layer. The existence of this oxide layer can improve the absorption rate of steel powder and is beneficial to their SLM process.

Table 3 Material parameters for the AM simulation of C300 powder

Parameters	Value
Powder Absorptivity	0.8
Solid Absorptivity	0.5
Thermal Expansion Coefficient (K ⁻¹)	10.0×10 ⁽⁻⁶⁾
Elastic Modulus (GPa)	175
Poisson Ratio	0.3
Material Yield Strength (MPa)	1050
Hardening Factor	0.03
Support Yield Strength Ratio	0.9
Powder Temperature (°C)	30°
Powder Convection Coefficient (W/mm ² °C)	200

2.3 AM Simulation Process of ANSYS

The metal AM process simulation process is largely divided into a geometry design and an additive process. The shape design simulation simulates a process of designing an over designed shape into a physically or structurally optimized shape and then validating it. AM build-up process analysis, and material characteristics and microstructure analysis. An example of AM process simulation workflow using ANSYS Additive Suite is shown in Fig. 3. The AM simulation processor using the Additive Suite first optimizes the shape to be additively manufactured using the Topology Optimization tool, and simulates the additive manufacturing (build-up)

process using the Additive Workbench or Additive Print tool.

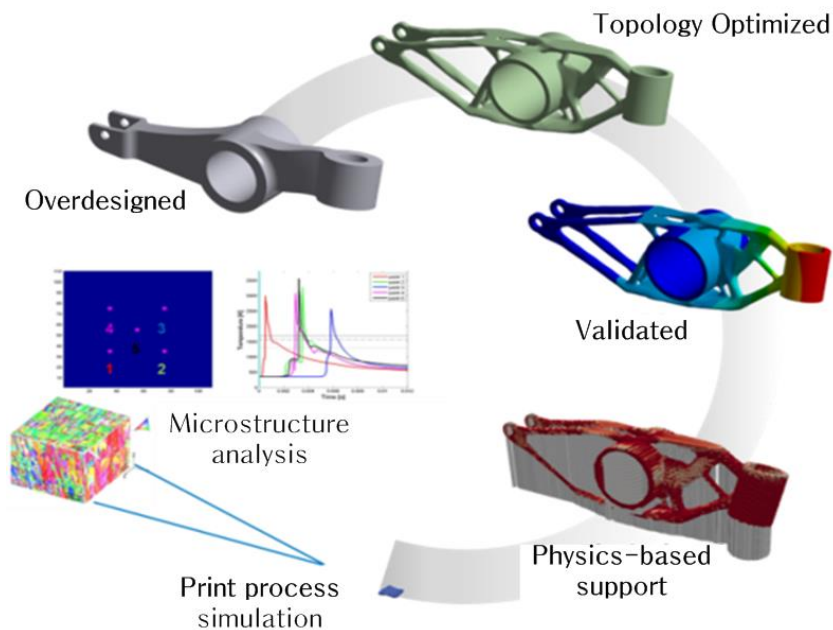


Fig. 3 AM process simulation flow chart with ANSYS Additive Suite [39]

On the other hand, it is also necessary to simulate preferentially using Additive Science to analyze the properties of additive manufacturing powder materials. The AM process simulation processor using ANSYS Additive Suite is shown in Fig. 3. By using Topology Optimization, static structural analysis is first performed after loading conditions are applied to the overdesigned shape [40],[41]. Based on this, a topology (physical or structural) optimization simulation is performed by determining the allowable range for optimization elements (mass, deformation, etc.) in the topology optimization environment. In addition, the stack shape is determined after a verification process through another static structural analysis. AM process simulation using Additive Workbench consists of supporter analysis, thermal analysis and structural analysis. Settings for these simulation processors can be easily accessed using the

Additive Wizard in the workbench. The steps for AM simulation in the workbench consist of 12 steps, including using the Additive Wizard to set process parameters. These simulation steps include the creation of an analysis system, definition of the additive material, mesh for the additive shape using the Additive Wizard, contact, supporter, material properties, process conditions, equipment conditions, temperature conditions, and the build-up process. Based on this, the results are analyzed through transient thermal and structural simulation.

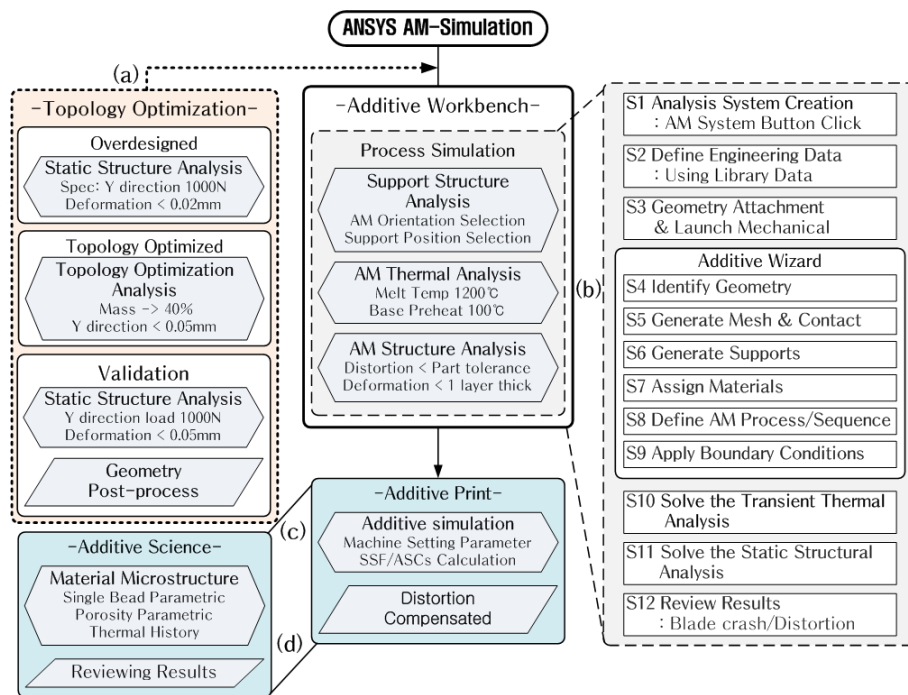


Fig. 4 AM process simulation processor using ANSYS Additive Suite

The AM simulation process using the Additive Workbench is shown detail in Fig. 4 (b). AM processor simulation using Additive Print is performed for the shape build-up process considering static structural analysis and transient thermal analysis. In addition, a simulation for easily determining the strain scaling factor (SSF) and anisotropic strain coefficients (ASCs) for the material is included. The AM simulation

process using the Additive Print is shown detail in Fig. 4 (c).

There are three types of Additive Print AM simulation: Assumed Strain simulation, Scan Pattern simulation and Thermal Strain simulation. The AM simulation processor using Additive Print is shown more detail in Fig. 5.

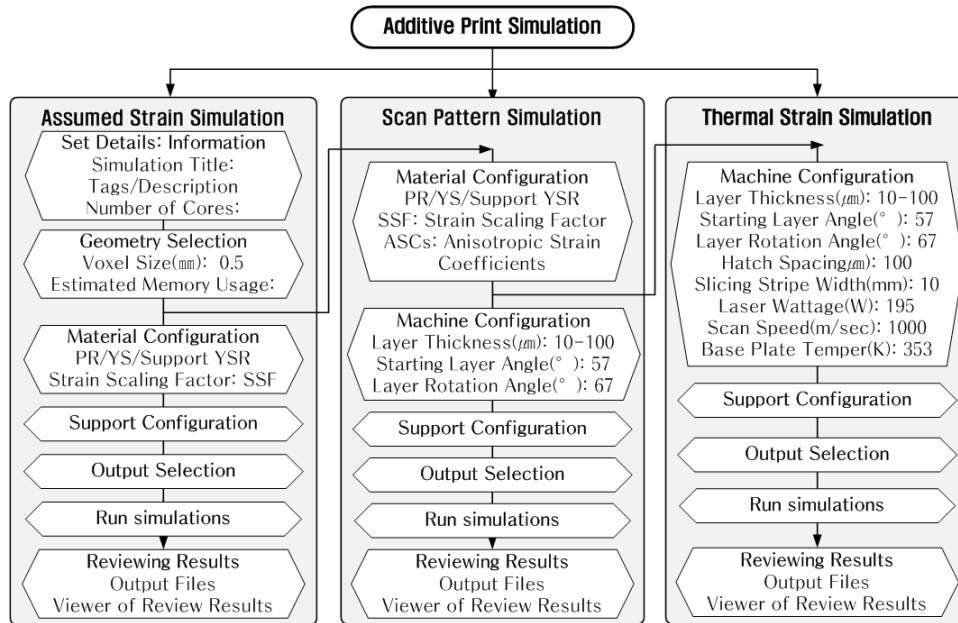


Fig. 5 AM simulation processor using Additive Print

The Assumed Strain simulation assumes that constant isotropic deformation occurs at all positions inside the part, and the fastest simulation is possible. The Scan Pattern simulation uses the same average strain size as the assumed uniform strain, but the simulation time increases as the strain for each component is subdivided according to the local direction of the scan vector within the part. The thermal strain simulation predicts how the thermal cycle affects the strain accumulation at each location in the part, and therefore requires the longest computation time for the simulation because it requires thermal prediction for all scan vectors. Calibration of SSF and ASCs

coefficients using Additive Print consists of a calculation process and a verification process. In this process, the coefficients are determined by comparing and analyzing the simulation results, and the measurement results obtained through actual production using 3D printing equipment.

2.4 Extracting Distortion Data

Distortion data extraction should be made from the AM Sample measurement and the simulated geometry measurement. This must be measured respectively for the case where it is manufactured and simulated according to the scan pattern. And it should be done in two cases, the supporter maintained condition and the removed condition. A schematic representation of the distortion data extraction method is shown in Fig. 6 and Fig. 7, respectively. Fig. 6 represents the coordinates of the position points for distortion measurement, and Fig. 7 represents the distortion measurement method before and after removal of the support.

The data point coordinates at the locations of interest, as shown in Fig. 6 are: Measurement A: (0, 5, 8.5) to (0, 5, 12.5) Use X-displacement value, Measurement B: (0, 5, 12.5) to (50, 5, 12.5) Use Z-displacement value. The distortion on measurement A is the maximum X-displacement value. The distortion on measurement B is the maximum Z-displacement value at $X = 50$ mm.

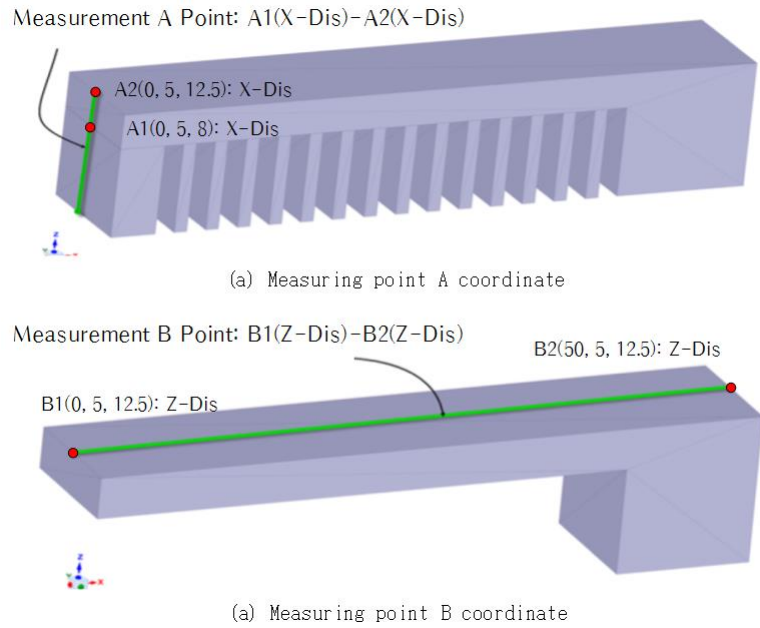


Fig. 6 Schematic of the point coordinates for the distortion measurement

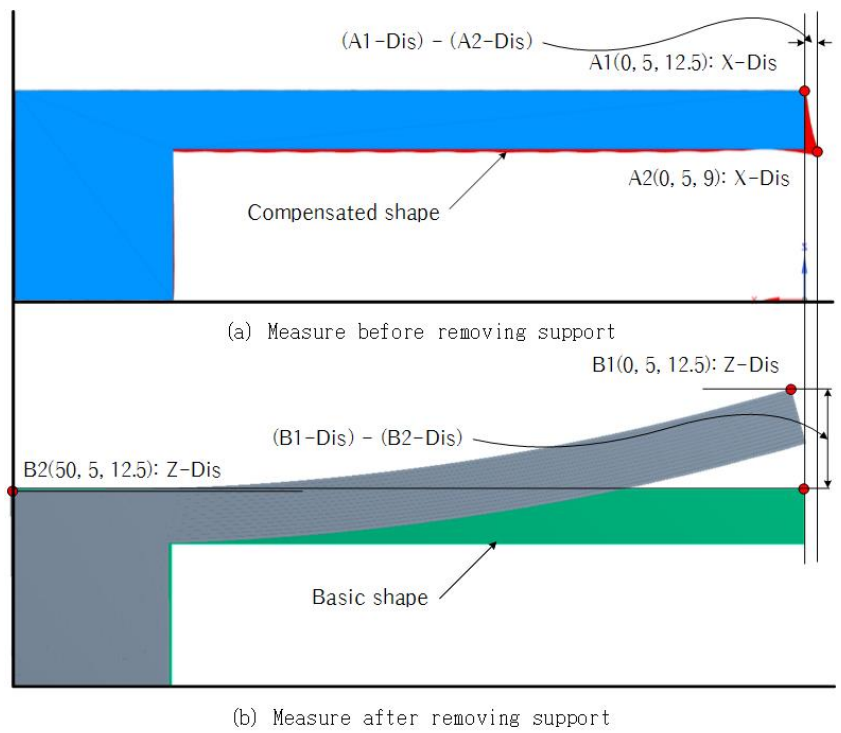


Fig. 7 Schematic of the distortion data extraction method

2.5 Scaling Factor Calculation

The simulation process of SSF and ASC calibration is as follows: input shape information, input support information, input material attribute information, input

device parameters and simulation result output settings. The parameters for materials and equipment for the SSF and ASC calibration simulations are the same as those applied to the AM sample preparations. The voxel size is defined as 0.25 mm. Depending on the size of the voxel, the simulation may not be possible due to insufficient memory. SSF and ASC calculations follow the process flow of Fig. 8.

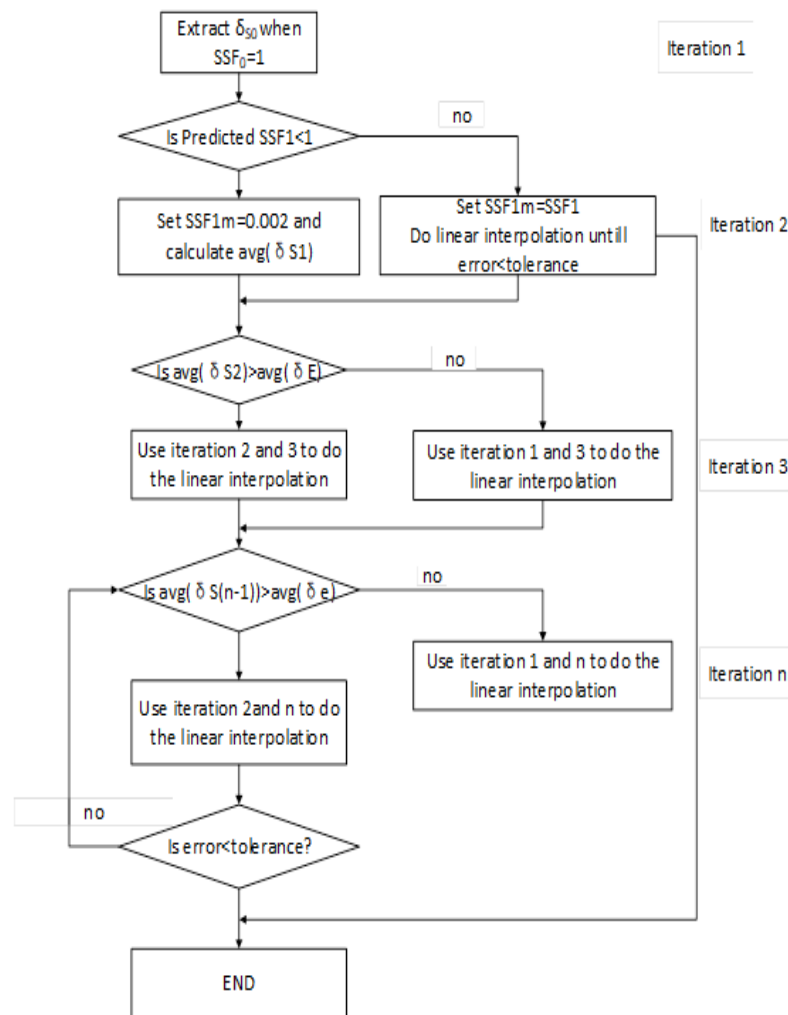

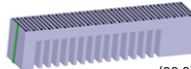


Fig. 8 Process flow for the SSF and ASCs calculations [38]

The calculation of the scaling factor follows the format of the spreadsheet provided by ANSYS. And an example of a spreadsheet for calculating the scaling fact is shown in Table 4. The variables and subscripts displayed in the spreadsheet are the same as in

Table 5. The first step of the simulation sets up the first iteration of the simulation using the following default values: In Assumed Strain mode, set as $SSF_0 = 1$, In Scan Pattern /Thermal Strain mode, set as $SSF_0 = 1$, $ASC_{||0} = 1.5$, $ASC_{\perp 0} = 0.5$.

Table 4 Spreadsheet for calculating scaling factors (case of Scan Pattern) [38]

SSF and ASCs Calibration for Scan Pattern Simulations										
Geometry Measurements			Distortion (mm)							
direction			$\delta e_{ }$							
⊥ direction			δe_{\perp}							
Extract distortion value at the location of interest from models built with scan patterns 1 and 2 (and B)										

	Simulation iteration	Simulation number		Distortion (mm)	Simulation settings			New settings			Error%
					SSF	ASC	ASC ⊥	SSF	ASC	ASC ⊥	
Linear Elastic	1st	n=0	direction	$\delta s_{ 0}$	SSF ₀	ASC ₀	ASC _{⊥0}	(E1) SSF ₁	(E2) ASC ₁	(E3) ASC _{⊥1}	(E4)ER ₁
		n=0	⊥ direction	$\delta s_{\perp 0}$							(E5)ER _{⊥1}
	2nd	n=1	direction	$\delta s_{ 1}$	(E1) SSF ₁	(E2) ASC ₁	(E3) ASC _{⊥1}	(E6) SSF ₂	(E7) ASC ₂	(E8) ASC _{⊥2}	(E9)ER ₂
		n=1	⊥ direction	$\delta s_{\perp 1}$							(E10)ER _{⊥2}
	3rd	n=2	direction	$\delta s_{ 2}$	(E6) SSF ₂	(E7) ASC ₂	(E8) ASC _{⊥2}	(E11) SSF ₃	(E12) ASC ₃	(E13) ASC _{⊥3}	(E14)ER ₃
		n=2	⊥ direction	$\delta s_{\perp 2}$							(E15)ER _{⊥3}
	4th	n=3	direction	$\delta s_{ 3}$	(E11) SSF ₃	(E12) ASC ₃	(E13) ASC _{⊥3}	:	:	:	:
		n=3	⊥ direction	$\delta s_{\perp 3}$:
	5th	n=4	direction	$\delta s_{ 4}$:	:	:	:	:	:	:
		n=4	⊥ direction	$\delta s_{\perp 4}$:

Table 5 Variable & Subscripts of spread sheet

Variable & Subscript	Meaning
δ_e	Experimental distortion
δ_s	Simulation distortion
r	Ratio
	Parallel to the scan direction
⊥	Perpendicular to the scan direction
n - 1	Setting before the most recent iteration
n	Setting of the most recent iteration
n + 1	Setting for the next iteration
0, 1, 2, ...	iteration 1, iteration 2, iteration 3, ...
m	Modified version

In the case of Assumed Strain mode, the target distortion value δ_{s_0} is extracted from the first stage simulation result. In the case of Scan Pattern/Thermal Strain mode,

the target distortion value $\delta_{S_{0\parallel}}$ is extracted from the first simulation and $\delta_{S_{0\perp}}$ is extracted from the second simulation. Scaling factor is calculated sequentially as indicated in the spreadsheet Table 4. After the initial value simulation, new SSF_1 and $ASC_{\parallel 1}$, $ASC_{\perp 1}$ are calculated, and after the next simulation, new SSF_2 and $ASC_{\parallel 2}$, $ASC_{\perp 2}$ are calculated.

In Assumed Strain mode, the SSF and ER (Error Rate) is calculated as follows:

$$SSF_1 = \frac{\delta_e}{\delta_{S_0}}, \quad SSF_0 \cong 0.1 \quad (\text{select a large value}) \quad (\text{A1})$$

$$ER_1 = \frac{|\delta_{S_0} - \delta_e|}{\delta_e} \quad (\text{A2})$$

In Scan Pattern/Thermal Strain mode, the SSF, ASCs and ER is calculated as follows:

$$SSF_1 = \frac{\delta_{e\parallel} + \delta_{e\perp}}{\delta_{S_{\parallel 1}} + \delta_{S_{\perp 1}}}, \quad SSF_0 \cong 0.1 \quad (\text{select a large value}) \quad (\text{E1})$$

$$ASC_{\parallel 1} = \frac{2}{\left(1 + \frac{\delta_{e\perp}}{\delta_{e\parallel}}\right)} \cong 1.999 \quad (\text{select a small value}) \quad (\text{E2})$$

$$ASC_{\perp 1} = 2 - ASC_{\parallel 1} \quad (\text{E3})$$

$$ER_{\parallel 1} = \frac{|\delta_{S_{\parallel 1}} - \delta_{e\parallel}|}{\delta_{e\parallel}} \quad (n \geq 1) \quad (\text{E4})$$

$$ER_{\perp 1} = \frac{|\delta_{S_{\perp 1}} - \delta_{e\perp}|}{\delta_{e\perp}} \quad (n \geq 1) \quad (\text{E5})$$

In the second step, after the first iteration simulation, the new SSF and ASC are calculated as follows.

In Assumed Strain mode, the SSF and ER (Error Rate) is calculated as follows:

$$SSF_2 = \frac{\delta_e}{\delta_{S_1}}, \quad SSF_1 \cong 0.1 \quad (\text{select a large value}) \quad (\text{A3})$$

$$ER_2 = \frac{|\delta_{S_1} - \delta_e|}{\delta_e} \quad (\text{A4})$$

In Scan Pattern/Thermal Strain mode, the SSF, ASCs and ER is calculated as

follows:

$$SSF_2 = \frac{\delta_{e_{\parallel}} + \delta_{e_{\perp}}}{\delta_{S_{\parallel 2}} + \delta_{S_{\perp 2}}}, \quad SSF_1 \doteq 0.1 \quad (\text{select a large value}) \quad (\text{E6})$$

$$ASC_{\parallel 2} = \frac{2}{\left(1 + \frac{\delta_{e_{\perp}}}{\delta_{e_{\parallel}}}\right)} \doteq 1.999 \quad (\text{select a small value}) \quad (\text{E7})$$

$$ASC_{\perp 2} = 2 - ASC_{\parallel 2} \quad (\text{E8})$$

$$ER_{\parallel 2} = \frac{|\delta_{S_{21}} - \delta_{e_{\parallel}}|}{\delta_{e_{\parallel}}} \quad (n \geq 1) \quad (\text{E9})$$

$$ER_{\perp 2} = \frac{|\delta_{S_{\perp 2}} - \delta_{e_{\perp}}|}{\delta_{e_{\perp}}} \quad (n \geq 1) \quad (\text{E10})$$

In the third step, after the second iteration simulation, the new SSF and ASC are calculated as follows.

In Assumed Strain mode, the SSF and ER (Error Rate) is calculated as follows:

$$SSF_3 = \frac{\delta_e}{\delta_{S_2}}, \quad SSF_2 \doteq 0.1 \quad (\text{select a large value}) \quad (\text{A5})$$

$$ER_3 = \frac{|\delta_{S_1} - \delta_e|}{\delta_e} \quad (\text{A6})$$

In Scan Pattern/Thermal Strain mode, the SSF, ASCs and ER is calculated as follows:

$$SSF_3 = \frac{\delta_{e_{\parallel}} + \delta_{e_{\perp}}}{\delta_{S_{\parallel 3}} + \delta_{S_{\perp 3}}}, \quad SSF_2 \doteq 0.1 \quad (\text{select a large value}) \quad (\text{E11})$$

$$ASC_{\parallel 3} = \left(\frac{\delta_{e_{\parallel}}}{\delta_{e_{\perp}}} - \frac{\delta_{e_{\parallel 1}}}{\delta_{e_{\perp 1}}} \right) \frac{(ASC_{\parallel 1} - ASC_{\parallel 0})}{\left(\frac{\delta_{e_{\parallel 2}}}{\delta_{e_{\perp 2}}} - \frac{\delta_{e_{\parallel 1}}}{\delta_{e_{\perp 1}}} \right)} + ASC_{\parallel 0} \doteq 1.999 \quad (\text{E12})$$

$$ASC_{\perp 3} = 2 - ASC_{\parallel 3} \quad (\text{E13})$$

$$ER_{\parallel 3} = \frac{|\delta_{S_3} - \delta_{e_{\parallel}}|}{\delta_{e_{\parallel}}} \quad (n \geq 1) \quad (\text{E14})$$

$$ER_{\perp 3} = \frac{|\delta_{S_{\perp 3}} - \delta_{e_{\perp}}|}{\delta_{e_{\perp}}} \quad (n \geq 1) \quad (\text{E15})$$

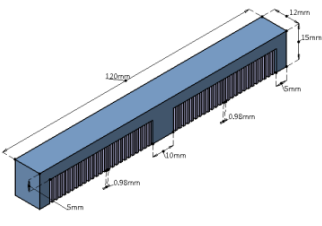
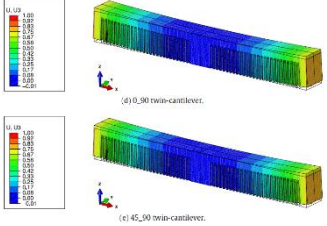
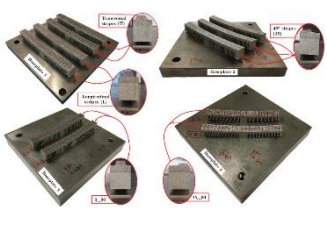
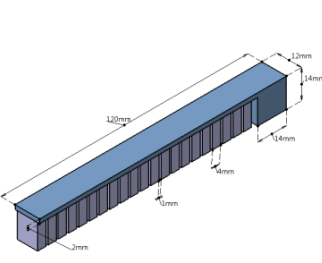
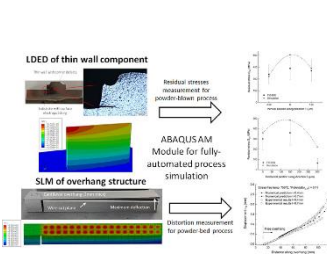
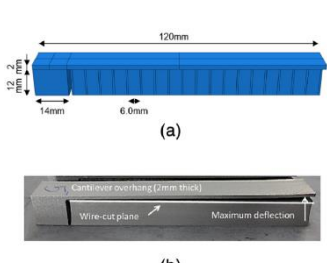
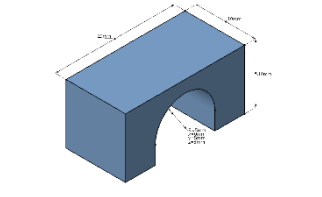
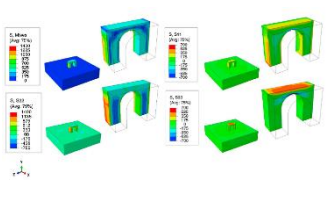
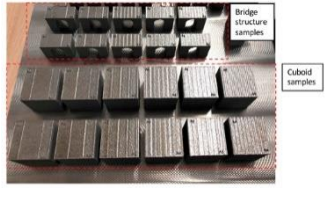
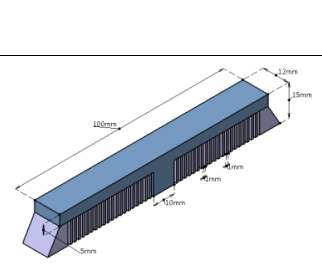
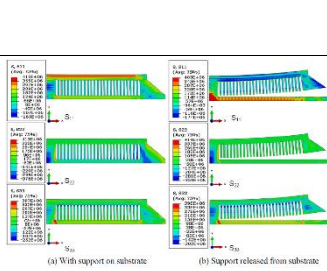
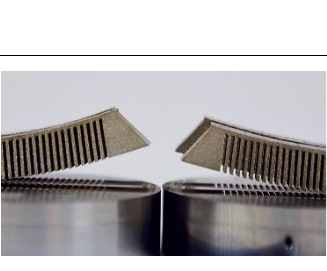
Chapter 3 AM Simulation Geometry Review

The shape of the product to be applied to the additive manufacturing process is very complex, and it is the case that difficult to manufacture by cutting or classical techniques. Even in AM process simulation, in order to achieve the purpose of the simulation, it is necessary to deal with a shape close to the actual product, not a simple shape. In other words, it is necessary to study the generalization of the layered shape in AM process simulation. In general, the additive manufacturing shape is composed of various geometries. Residual stresses or distortions in additive manufacturing products will be generated by geometric interactions composed of various shapes. Therefore, in order to further increase the accuracy of shape correction in AM simulation software, it is desirable to correct the SSF and ASC coefficients for the generalized shape. Here, the generalized shape means a sample shape that can respond to all additive manufacturing parts. That is, regardless of the shape, size, complexity, and difficulty of fabrication of the additive manufacturing parts, when a simulation is performed by applying a generalized shape, the result is a shape that can guarantee reliability. From this point of view, the existing AM simulation studies were investigated and the sample shape was analyzed. The shape of the AM simulation sample of the previous study is summarized in the Table 6.

As shown in previous AM simulation studies, the length is long and the shape is simple. Most of these shapes have a beam or bridge shape. These shapes seem to be because they are the simplest shapes in the additive manufacturing process and are easily deformed, and they are also shapes that allow easy measurement of distortion.

It can be seen that the existing AM simulation studies mainly consist of inherent strain, residual stress and distortion, and thermal compensation. This means that these factors cause the most problems in the manufacture of AM parts. That is, it can be seen that the key point to be solved in manufacturing AM parts is to minimize distortion due to residual stress. This problem can be solved by improving the additive manufacturing environment that minimizes residual stress or by compensating for the distortion of the AM shape by predicting the distortion in advance.

Table 6 Review of AM simulation sample shape in existing research

AM sample geometry	AM sample simulation	AM sample product	Remark
			[14] inherent strains
			[15] residual stresses and distortion
			[16] residual stress
			[17] residual stress

			<p>[18] distortion prediction</p>
			<p>[18] distortion prediction</p>
		<p>-</p>	<p>[19] thermal compensation</p>
		<p>-</p>	<p>[19] stress and distortion</p>
			<p>[20] distortion and cracking</p>
		<p>-</p>	<p>[21] distortion and residual stresses</p>

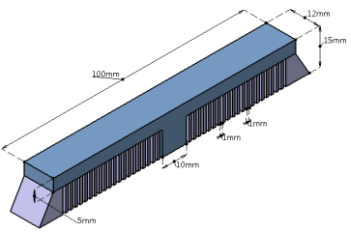
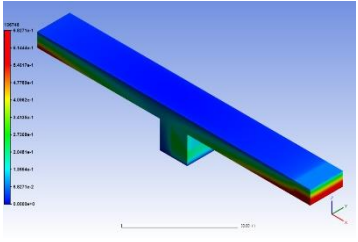
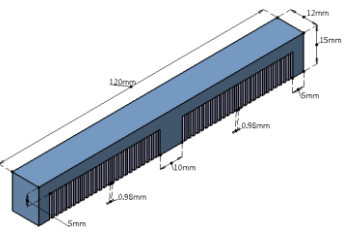
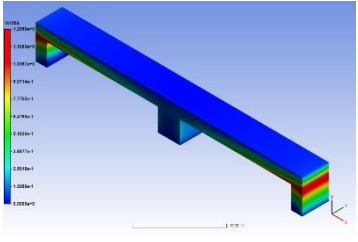
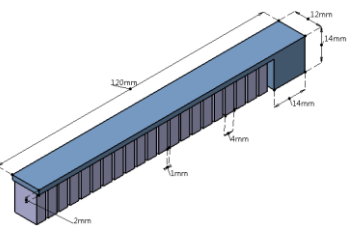
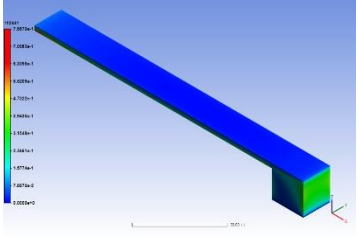
		-	[22] distortion prediction
			[23] residual stress and distortion
			[24] shape-distortion
<p>Fig. 3. FE models used for the numerical simulation of the AM process: (a) rectangular deposit on (b) Substrate deposition.</p>	<p>Fig. 14. Rectangular deposition Cosmographic Control prediction of distortion of size with experimental method.</p>		[25] residual stress and distortion
		-	[26] Residual deformation

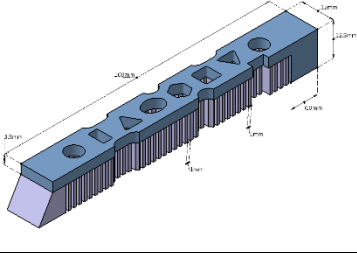
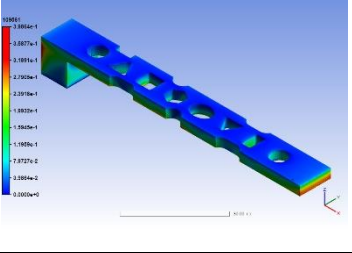
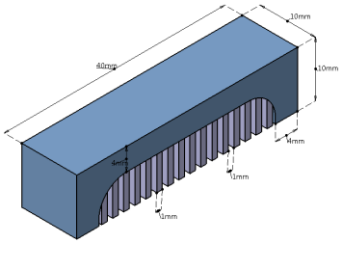
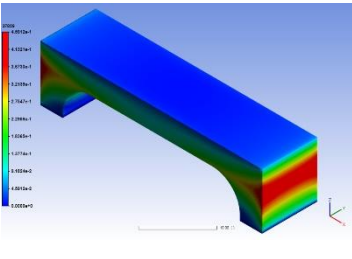
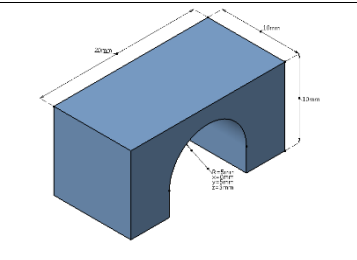
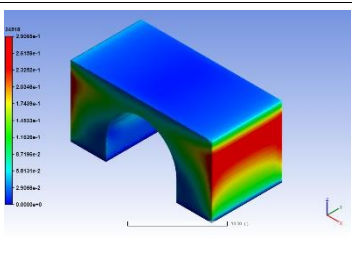
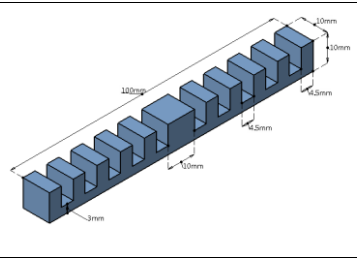
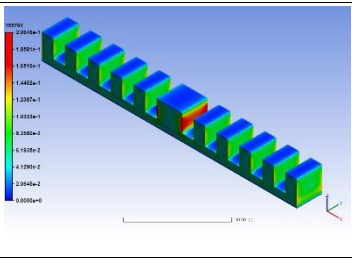
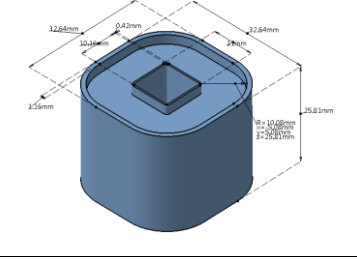
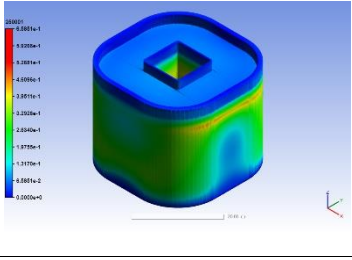
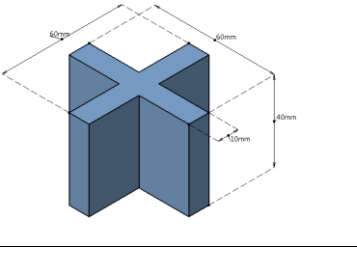
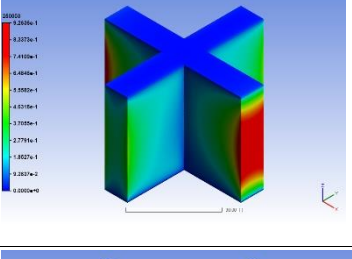
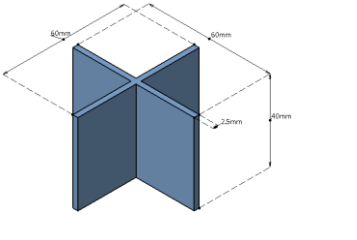
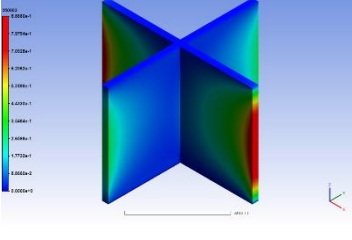
The AM simulation shapes that were applied in the previous study were reviewed through AM simulation analysis. The simulation mode was applied as Scan Pattern, and the scanning start and rotational angle were set to (0, 0). In this simulation result, the distortion represents the displacement in the longitudinal direction without removing

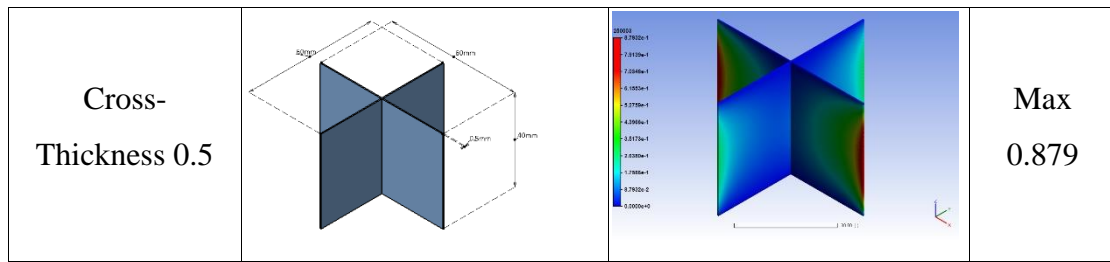
the supporter. The simulation results according to the shape of the AM sample are summarized in Table 7. Summarized in the simulation results for the AM simulation shapes applied in the previous study are as follows: The thinner the thickness of the AM sample shape end, the smaller the longitudinal distortion. The longer the length, the greater the distortion in the height direction. The larger the size of the part, the greater the distortion. The more complex the shape, the smaller the distortion.

As described above, specificity was shown according to the shape of the AM sample, but no significant singularity was found for the criteria of selection for the AM sample.

Table 7 Simulation result according to AM sample geometry

Shape Type	AM sample geometry	Simulation result	Distortion
Twin-Cantilever-Beam-100mm			Max 0.683
Twin-Support-Cantilever Beam-120mm			Max 1.296
Cantilever-Beam-120mm			Max 0.789

<p>Mix type Cantilever Beam-100mm</p>			<p>Max 0.399</p>
<p>Bridge 40mm</p>			<p>Max 0.459</p>
<p>Bridge 20mm</p>			<p>Max 0.291</p>
<p>Block array- 100mm</p>			<p>Max 0.206</p>
<p>Canonical- Square (25.5x32.6x32.6)</p>			<p>Max 0.659</p>
<p>Cross- Thickness 10</p>			<p>Max 0.926</p>
<p>Cross- Thickness 2.5</p>			<p>Max 0.887)</p>



The possibility to generalize the shape of the AM sample was examined by including all the basic geometric shapes that make up the shape of the AM sample. After redesigning the shape of the AM sample suggested in the previous study, and performing simulation using Additive Print, the distortion was measured. The simulation was performed for three methods: Assumed Strain, Scan Pattern, and Thermal Strain. And the parameters of the machine and the material were performed under the same conditions. The simulation results according to the AM shape and simulation mode are summarized in Table 8.

And the graph of the maximum distortion according to the AM shape and AM simulation mode is shown in Fig. 9. The influence on distortion according to AM sample shape and simulation mode is as follows: Distortion is greatly affected by the scan pattern. It is affected by length. It is affected by the cooling area. There is little effect on the complexity of the shape. Solid type is more affected than latex type. The thicker the thickness, the more affected. It was found that the effect of distortion was more influenced by thermal stress than geometric shape, and most affected by scan pattern than thermal stress. As a result, the necessity for generalization of sample shape for AM simulation could not be confirmed.

Table 8 AM simulation result according to AM shape and simulation mode

	Assumed Strain	Scan Pattern	Thermal Strain
Model 1 (Basic Len-50)			
Model 2 (Len-100)			
Model 3 (Len-100)			
Model 4 (Len-100)			
Model 5 (Len-100)			
Model 6 (Len-100)			

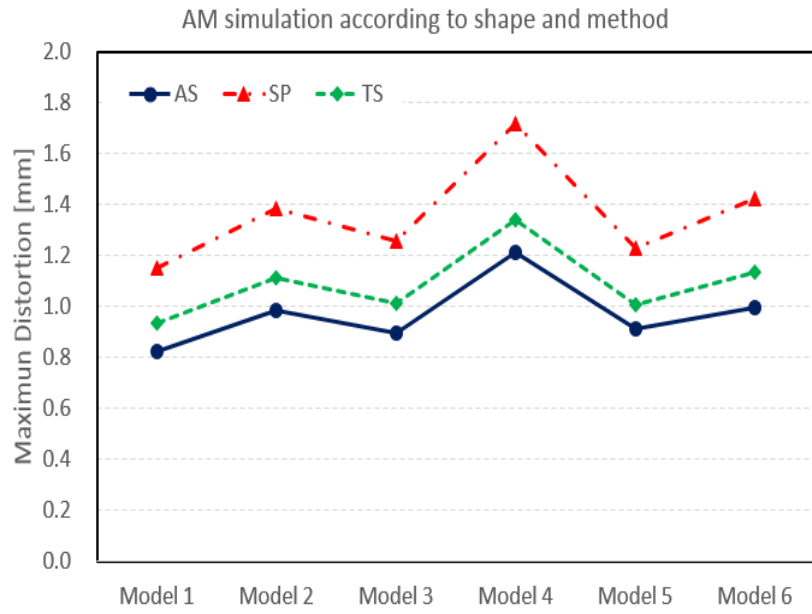


Fig. 9 Maximum distortion according to AM shape and AM simulation mode

Chapter 4 Experiment

4.1 AM Sample Geometry

Cantilever beam sample shape file and corresponding supporter as STL format be provided. AM sample dimensions (50 x 10 x 12.5 mm) are shown in Fig. 10. The sample and the corresponding supporter are marked together in Fig. 11, and the red dotted line indicates the supporter cutoff position.

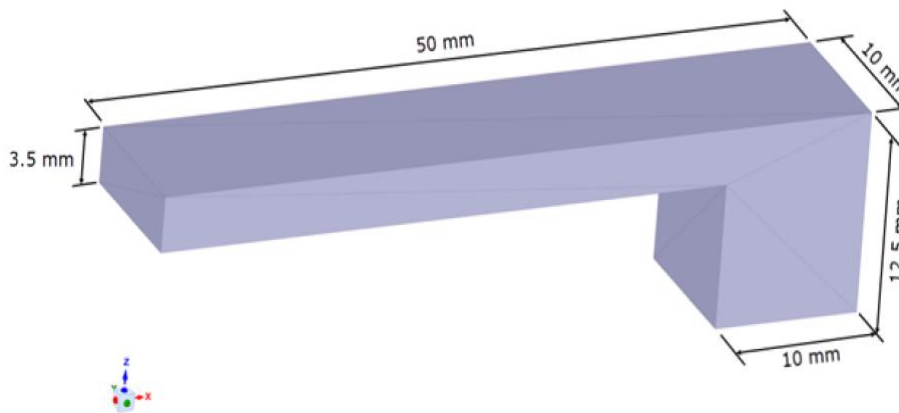


Fig. 10 Cantilever beam dimensions [38]

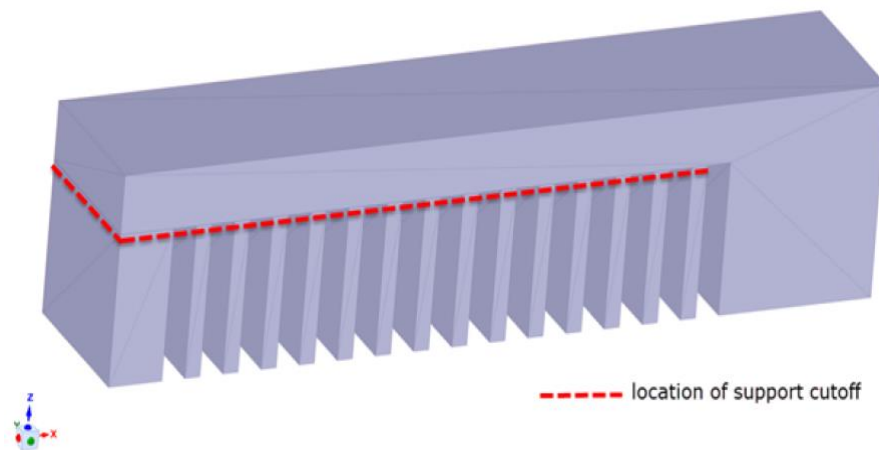


Fig. 11 Cantilever beam with support[38]

4.2 AM Sample Manufacture

4.2.1 Parts Layout

AM samples for calibration must be built on the same base plate. This is because three cantilever beam samples with different scan patterns must be manufactured under the same conditions. The layout of the AM sample should be implemented in consideration of the gas flow direction. It is necessary to ensure that there is sufficient measurement space between the parts before cutting the AM sample on the base plate. Since AM samples should be measured while fixed to a plate, consideration should be given to maintaining sufficient space between adjacent samples. The layout according to the scan pattern for additive manufacturing of AM sample is shown in the Fig. 12.

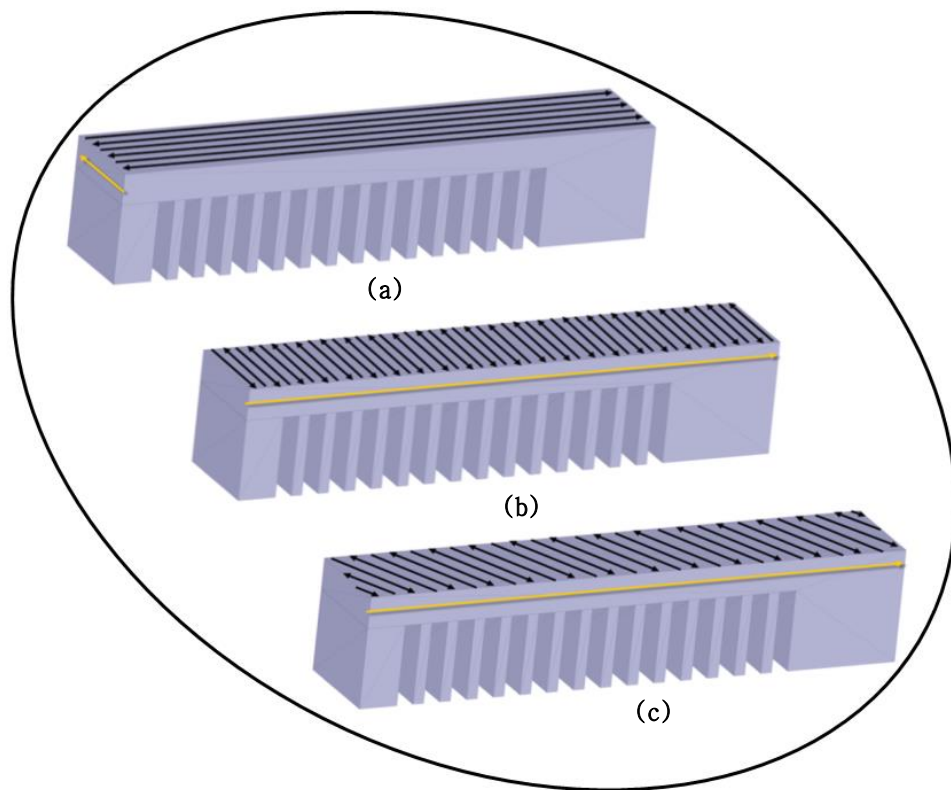


Fig. 12 Layout of AM sample for the additive manufacturing

A detailed description of the scan patterns (a), (b), and (c) shown in Fig. 12 is as follows:

Scan Pattern (a): Bi-directional scan with a starting angle of 0° and a layer rotation angle of 0° . The scan line is 0° or 180° . (See Fig. 13)

Scan Pattern (b): Bi-directional scan with a starting angle of 90° and a layer rotation angle of 0° . The scan line is 90° or 270° . (See Fig. 14)

Scan Pattern (c): Use the scan pattern you want to use to make the actual component. In this guide, we use a rotating stripe scan pattern with a starting angle of 0° and a rotation angle of 67° . (See Fig. 15)

Here, the angle represents the laser direction, not the stripe direction.. The X axis should always be parallel to the length of the cantilever. If the machine uses a different coordinate system, it should be checked that the scan pattern (a) ($0^\circ, 0^\circ$) makes the laser scan parallel to the length of the cantilever. To achieve this, it may be necessary to set the stripe width to be greater than or equal to the length of the cantilever (50 mm). For scan pattern (b) ($90^\circ, 0^\circ$), the stripe width should be set to be at least the cantilever width (10 mm).

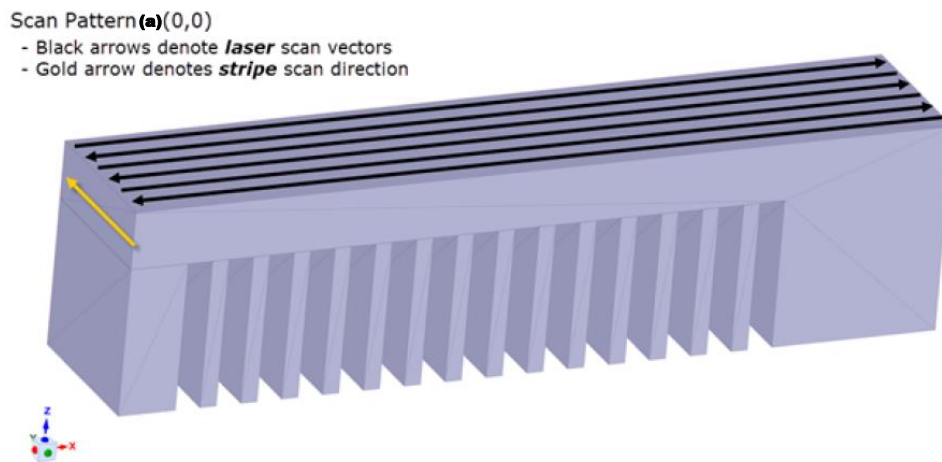


Fig. 13 Scan pattern (a) ($0^\circ, 0^\circ$) [38]

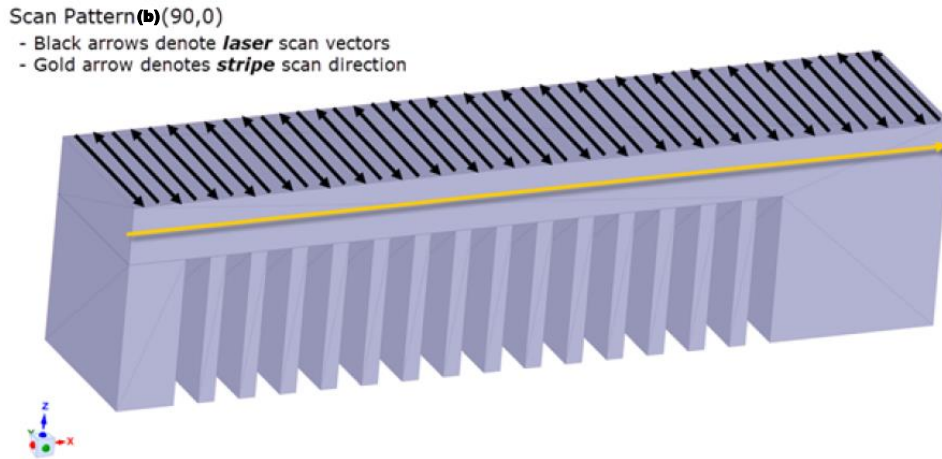


Fig. 14 Scan pattern (b) (90°, 0°) [38]

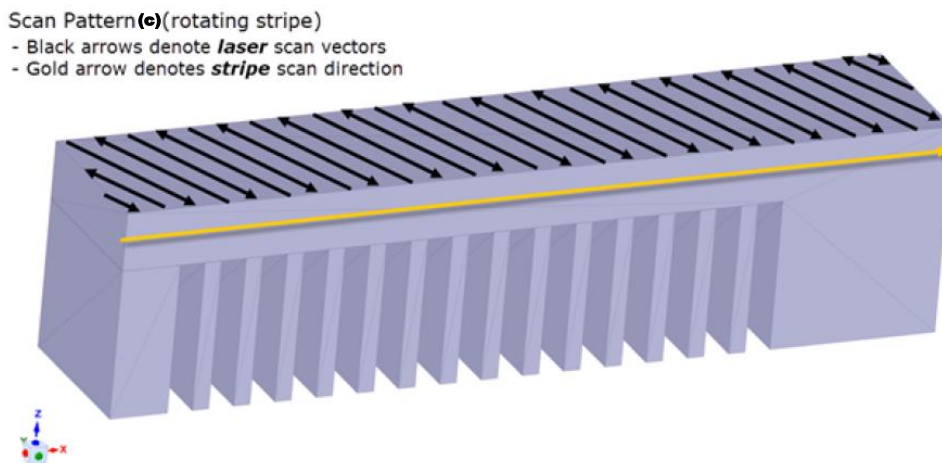


Fig. 15 Scan pattern (c) (rotating stripe) [38]

4.2.2 Build-up Parts

The metal 3D printer for the additive manufacturing of AM samples used Mx3 (WinForsys, Seoul Korea) equipment of the Powder Bed Fusion method. The build-up parameters for the materials and equipment of the additive manufacturing process applied optimized values provided by the manufacturer. The build-up parameters of additive manufacturing equipment used for AM sample manufacturing are shown in Table 9.

Table 9 Build-up parameters

Paremeter	Value WinForsys
Baseplate Temperature (°c)	50
Layer Thickness (µm)	30
Staring Layer Angle (°)	0,90,0
Layer Rotation Angle (°)	0,0,67
Hatch Spacing (µm)	70
Slicing Stripe Width (mm)	10
Laser power(W)	190
Scan Speed(mm/s)	1000
Powder Temperature(°c)	
Gas Temperature (°c)	
Gas Convection Coefficient (W/mm ² .°c)	



Fig. 16 AM Sample before wire cutting

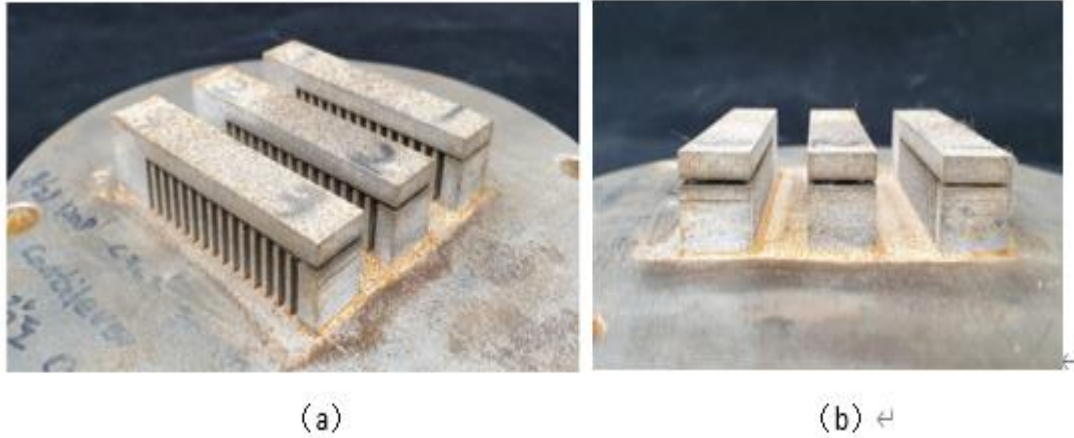


Fig. 17 AM Sample after wire cutting

Distortion measurement for AM samples for simulation of the scaling factor should be performed in two ways. One is the measurement of distortion in the condition before removing the support, and the other is the measurement of distortion in the condition after removing the support. The AM sample manufactured for distortion measurement is shown in Fig. 16 and Fig. 17. Fig. 16 shows the AM sample before wire cutting, and Fig. 17 shows the AM sample after wire cutting.

4.3 Taking Distortion Measurements

The measurement of distortion for the AM sample can be done in a variety of ways to obtain the best resolution. For this study, Vernier-calipers and 3D scanning method were used. The measurement of distortion by Vernier-calipers is summarized in Table 10. And the measurement of distortion by 3D scanning is summarized in Table 11. When using the Coordinate Measurement Method(CMM) by 3D scanning, many points along the selected surface of the cantilever beam are measured with lines. Find the maximum deflection for the measuring position.

Table 10 Distortion measurement of AM sample by vernier calipers

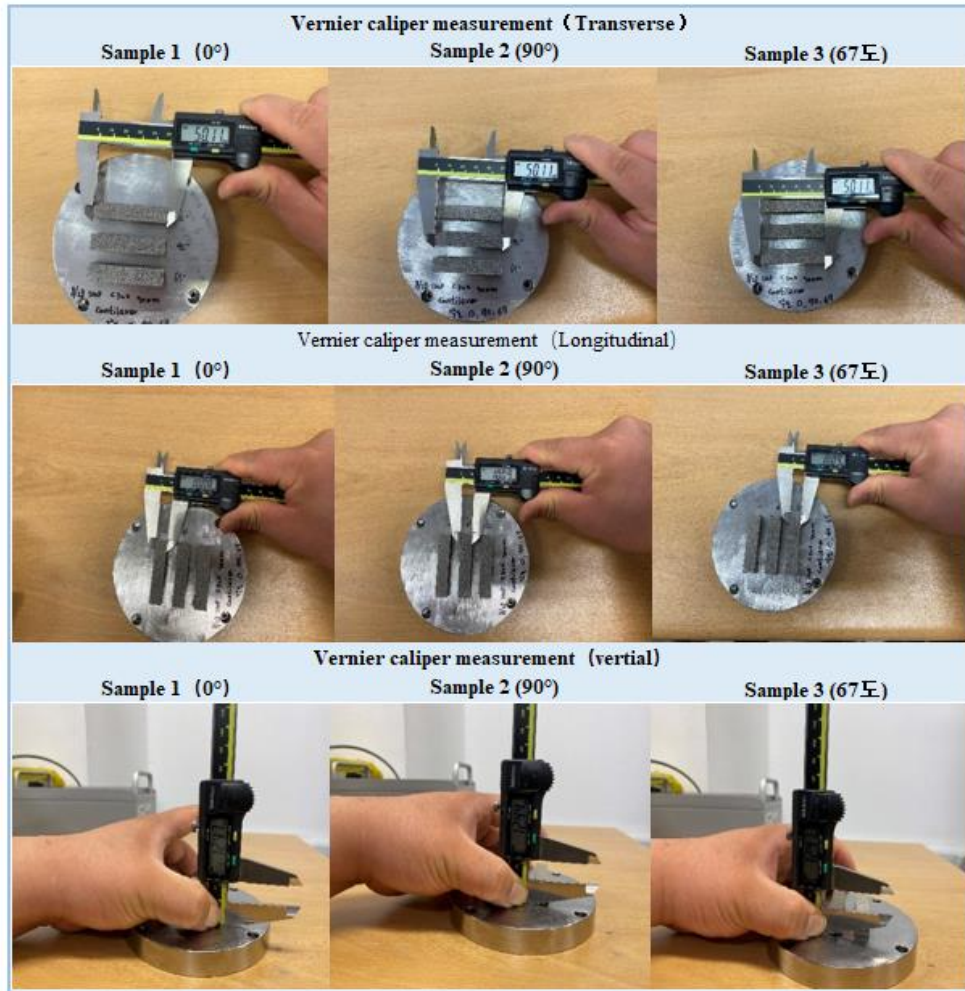
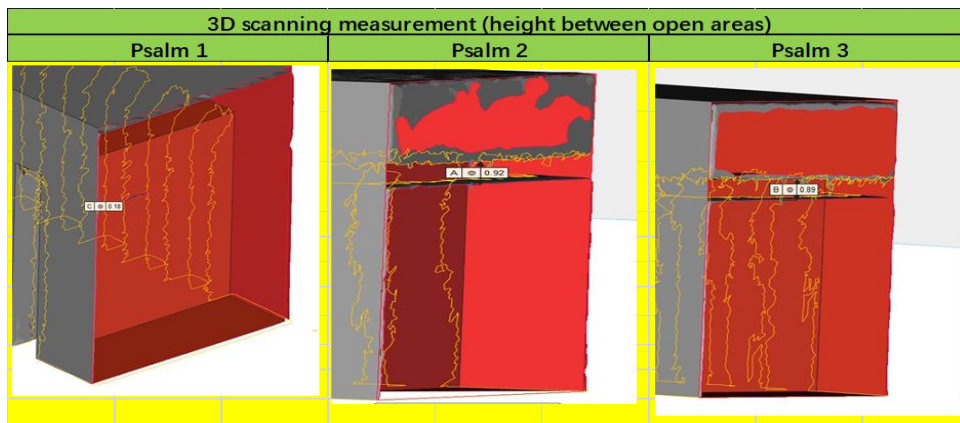


Table 11 Distortion measurement of AM sample by 3D scanning



The maximum X-deformation of measurement a usually occurs at the interface

between the beam and the support, but it is good practice to compare the measurements along the height. Also, The maximum Z-strain of measurement usually occurs at the cantilevered beam end, but it is good practice to compare the measurements on the top surface.

If you are using a laser scanner you can get a point cloud or scanned STL file and measure the distortion at the X and Z positions of interest. The distortion measurement data of the AM sample by 3D scanning shows in Table 12.

Table 12 3D scan sample measurement results of point A and B

	Scan Pattern (a) (0°, 0°)	Scan Pattern (b) (90°, 0°)	Scan Pattern (c) (0°, 67°)
Z-distance: A (mm)	50.537	50.536	50.523
X-distance: B (mm)	12.68	13.42	13.39

4.4 Simulation approach

The Additive Manufacturing (AM) simulation software packages ANSYS Additive Print and ANSYS Additive Suite are intended to simulate the PBF process to avoid unplanned machine downtime and improve part quality. By predicting deformations and stresses in AM parts during the manufacturing process, these tools form the basis for assessing their design integrity. Residual deformations of AM components can be predicted and compensated prior to starting the actual manufacturing process. Especially, the corrected SSF and ASC using Additive Print significantly improve the calibration accuracy of the simulation software, not only

improving the chance of a successful build, but also reducing trial and error costs.

For this study ANSYS version 2020R1 was used. The software simulation procedures and methods described below follow the approach provided by ANSYS. The conditions and parameters for geometry, material, and machine used in the simulation setup were applied in the same as the AM sample production environment.

There are three types (Assumed Strain, Scan Pattern, or Thermal Strain) of simulation for Scaling Factor correction using Additive Print software. For this study the scan pattern type was mainly used.

The simulation setup screen for the scaling factor correction of Additive Print software shows in Fig. 18. In the Fig. 18 (a) and (b) show the imported status of the build parts and the support parts, respectively. As shown in (a) of Fig. 18, the Voxel Size selection of the build parts is directly related to the simulation failure and success. If the Voxel Size is too small, a lot of memory is required and the simulation takes a long time. Sometimes it can lead to simulation failure. When the Voxel Size is increased, the simulation time is short and the probability of success is increased. However, the accuracy is lowered. Voxel Size should be selected in consideration of user PC environment and simulation level. In this study, a Voxel Size of 0.25 mm was selected and applied.

In Additive Print simulation, the setting of Outputs is also a very important pointer. This is because the required output data may vary depending on the simulation purpose. In Additive Print simulation, Outputs can set the following items: On-plate residual stress/distortion, Supports residual stress/distortion, Distortion compensated STL file

(after cutoff), Layer by layer stress/distortion, ANSYS mechanical files to detect potential blade crashes due to distortion.

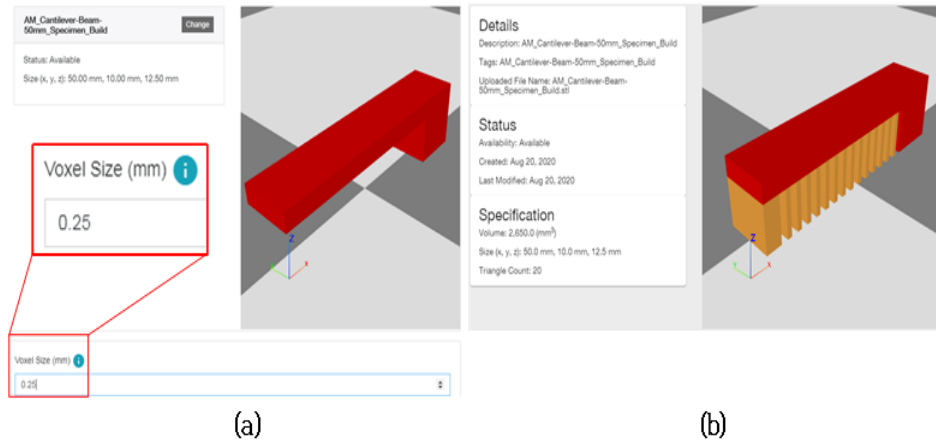


Fig. 18 Simulation setup screen for scaling factor correction

In Additive Print simulation, the setting of outputs is also a very important pointer. This is because the required output data may vary depending on the simulation purpose. In the Additive Print simulation, outputs is allowed to set the following items: On-plate residual stress/distortion, residual stress/distortion, Distortion compensated STL file (after cutoff), Layer by layer stress/distortion, ANSYS mechanical files, Detect potential blade crash due to distortion.

Simulation result data can be checked directly through a dedicated view as shown in Fig. 19 or can be analyzed externally by exporting it as a geometry file or raw data. Fig. 19 (a) and (b) show the distribution of stress and strain through a dedicated view, respectively. And (c) and (d) of Fig. 19 show examples of distorted pointer data and distortion-compensated surface data through an external analysis program of the extracted file, respectively. For this study, as an external analysis program to measure

distortion was used software ParaView.

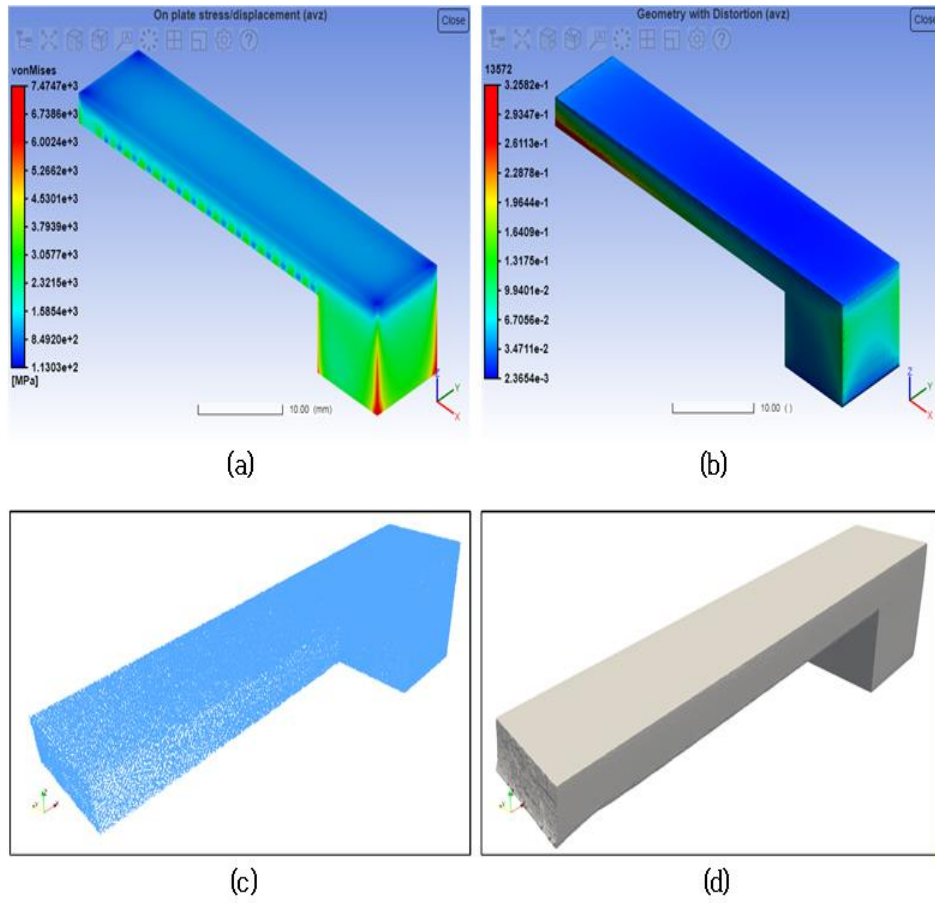


Fig. 19 Extract data from AM simulation outputs

Chapter 5 Results and discussion

5.1 Calibration of SSF and ASCs for the measurement Point A

According to simulate the manufacturing process of the printed model through the Assumed Strain mode, Scanning mode and Thermal Strain mode in the ANSYS analysis software. During the printing process, the layer transition angle was set to 0° , 90° , and 67° for simulation comparison. After simulating the analysis results of three models and three scanning angles, then compared with the actual sample, and measured the deformation values of point A and point B of the sample. Here, point A is the deformation value before the support is removed and point B is the deformation value after the support is removed.

The calculation of SSF and ASCs at Point A is as follows: In the Assumed Strain mode, the initial simulation was kept at a certain angle (starting angle 0, rotation angle 0) between layers without rotation using only one mode. The SSF result calibrated by Assumed Strain simulations based on the distortion value measured from the fabricated AM sample and the distortion value measured from the shape of the simulation result is shown in Table 13. When SSF is set to 1 for the first time, the deformation of point A obtained by simulation is 0.0266327 mm. After numerical optimization, the deformation of point A after the first macro-optimization is 0.437. (See Fig. 20) In the simulation process using the third scan mode, under the initial setting value, only small deformations of the two room-second modes are shown, which are 0.03798 mm and 0.015128 mm, but they also represent huge Simulation error. From Table 13, it can be seen that the error has decreased to 0.1% after performing two simulations.

Table 13 Calibration of SSF by Assumed Strain simulation

	Distortion (mm)
Geometry Nominal	
Measurement	0.4

Linear Elastic	Simulation iteration	Simulation number	Distortion (mm)	Simulation settings	New settings	Error%
				SSF	SSF	
	1st		0.0266327	1	16.4084	
2nd		0.437	16.4084	16.4084	0.0%	

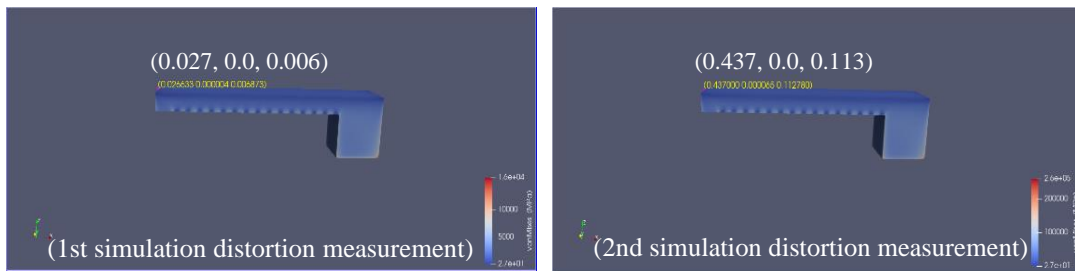


Fig. 20 Distortion of Assumed Strain simulation

In the scanning mode, the initial simulation was kept at a certain angle (starting angle 0, rotation angle 0) and (starting angle 90, rotation angle 0) using two mode. Table 14 shows the distortion value based on the distortion value measured from the manufactured AM sample and the distortion value measured from the shape of the simulation result, and SSF and ASC results calibrated by scanning simulation.

Table 14 Calibration of SSF and ASCs for Scan Pattern simulation

Geometry Measurements	Distortion (mm)		
direction	0.437		
⊥ direction	0.436		

Linear Elastic	Simulation iteration	Simulation number	Distortion (mm)	Simulation settings			New settings			Error%
				SSF	ASC	ASC ⊥	SSF	ASC	ASC ⊥	
	1st		direction	0.0379838	1.00	1.50	0.50	16.44	1.00	
		⊥ direction	0.015128							96.5%
2nd		direction	0.437841	16.44	1.00	1.00	16.39	1.00	1.00	0.2%
		⊥ direction	0.437841							0.4%
3rd		direction	0.44	16.39	1.00	1.00	16.44	1.00	1.00	0.1%
		⊥ direction	0.44							0.1%

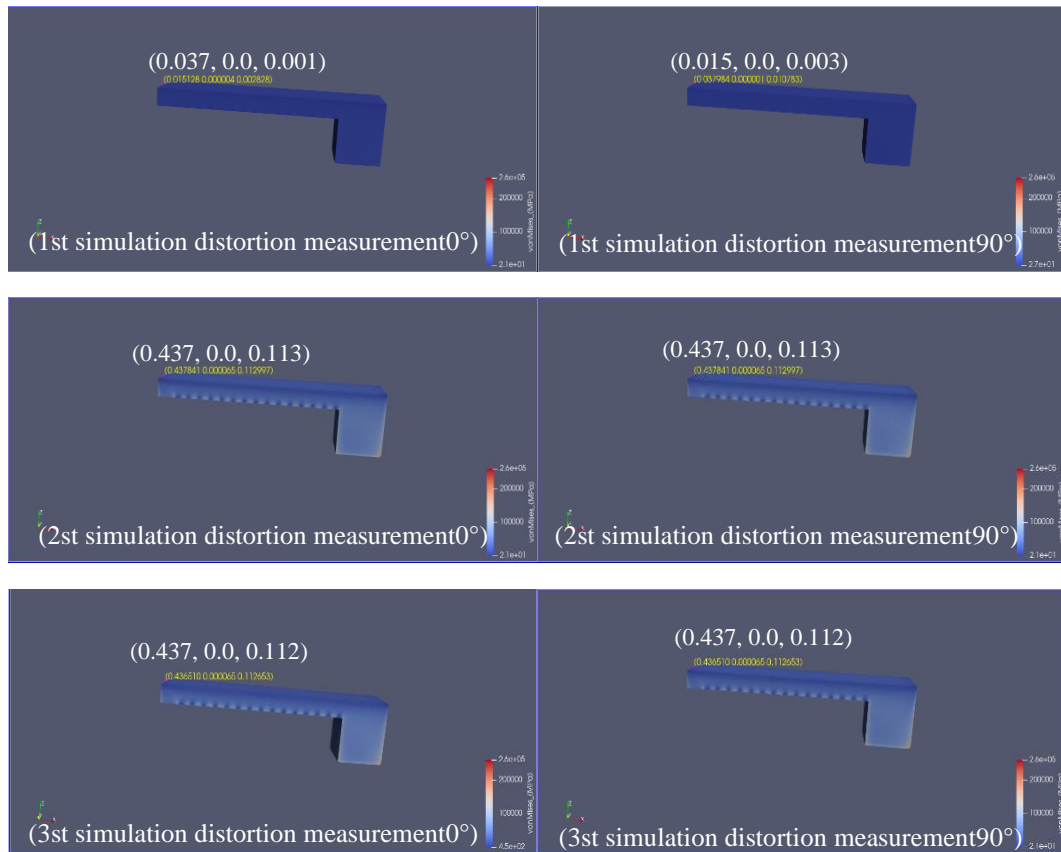


Fig. 21 Distortion of Scan Pattern simulation

In the thermal strain mode, the initial simulation was kept at a certain angle (starting angle 0° , rotation angle 0°) and (starting angle 90° , rotation angle 0°) using two modes. Table 15 shows the results of calibrating the results of SSF and ASC based on the thermal strain simulation based on the deformation values measured from the manufactured AM samples and the deformation values measured from the shape of the simulation results. A macro-optimization was performed in the thermal strain mode. It can be seen from Figure 22 that when the rotation angle between the layers is 0° , the obtained deformation is 0.437 mm, and the scanning angle between the layers is 90° , and the deformation measured at point A is 0.436 mm. Although different scanning modes will produce different thermal gradients and cooling rates, in the manufacture of C300

powder bed, the change of heat distribution does not affect the final deformation and has a great impact.

Table 15 Calibration of SSF and ASCs for Thermal Strain simulation

Geometry Measurements	Distortion (mm)		
∥ direction	0.437	Extract distortion value at the location of interest from models built with scan patterns 1 and 2 (∥ and ⊥)	
⊥ direction	0.436		

Linear Elastic	Simulation iteration	Simulation number	Distortion (mm)	Simulation settings			New settings			Error%
				SSF	ASC ∥	ASC ⊥	SSF	ASC ∥	ASC ⊥	
	1st		∥ direction	0.072601	1	1.5	0.5	8.6146	1.0011	0.9989
		⊥ direction	0.028739							93.4%
2nd		∥ direction	0.44	8.6146	1.0011	0.9989	8.5986	1.0048	0.9952	0.4%
		⊥ direction	0.44							0.8%

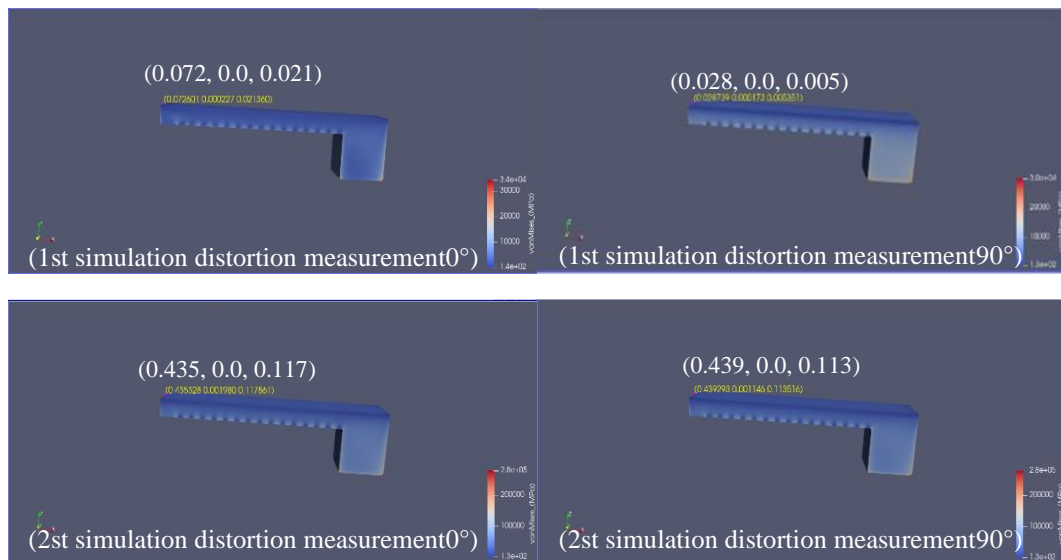


Fig. 22 Distortion of Thermal Strain simulation

In the initial simulation, the SSF and ASC values were set to 1, 1.5 and 0.5 respectively, which are the directions parallel and perpendicular to the scanning direction. Although the final deformation obtained in the two scanning modes is 0.072601 and 0.028739. But the simulation structure executed in this mode has larger errors, which are 83.4% and 93.4% respectively. However, when the interlayer is 0°,

the value of the ANSYS module seems to be much larger than the actual deformation, and the simulation result with a scanning angle of 90° between layers shows that the deformation is smaller than the actual value.

In the second simulation, a deformation of 0.44 mm was generated in both scanning modes. The error is reduced to 0.4%, and the optimized value will provide data support for the next step of fine optimization.

5.2 Fine calibration of SSF and ASCs for the measurement Point A

After using three deformation models to simulate the macro adjustment of SSF and ASCs parameters, the layer rotation is set to 67° to fine-tune the process parameters. While optimizing the process parameters, the deformation result is closer to the true value.

The calculation of SSF and ASCs fine-tuning at Point A is as follows: In the assumed strain mode, only one mode is used to maintain the initial simulation at a specific angle between the layers (starting angle 0, rotation angle 67°) without rotating. The SSF result calibrated by Assumed Strain simulations based on the distortion value measured from the fabricated AM sample and the distortion value measured from the shape of the simulation result is shown in Table 16. In the process of using micro-control, the deformation amount is assumed to be 0.423 mm in the strain model with 67° rotation between layers. Compared with 0.437 mm after the first optimization, the obtained deformation is closer to the actual value, and the reference value is set. (See Figure 23)

Table 16 Calibration of SSF for Assumed Strain simulations

	Distortion (mm)
Geometry Nominal	
Measurement	0.423

Linear Elastic	Simulation iteration	Simulation number	Distortion (mm)	Simulation settings	New settings	Error%
				SSF	SSF	
	1st		0.437	16.41	15.88	3.3%
2nd			0.422927	15.88	15.89	0.0%

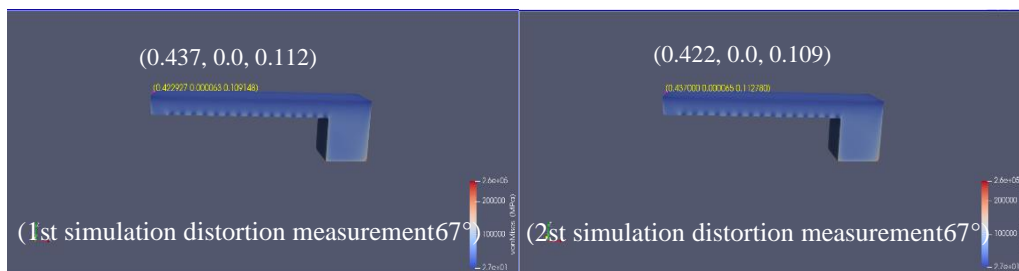
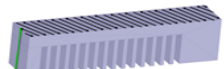


Fig. 23 Fine tuning distortion of Assumed Strain simulations

In the Scan Pattern mode, only one mode can be used to maintain the initial simulation at a specific angle between the layers (starting angle 0, rotation angle 67) without rotation. Table 17 shows the SSF results based on the scan mode simulation calibration based on the distortion value measured from the manufactured AM sample and the distortion value measured from the shape of the simulation result. In the scan mode, use the interlayer scan rotation 67° for simulation, and use the first optimized SSF and ASC values of 16.44, 1.00 and 1.00 for the third simulation process optimization. The final deformation is 0.42 mm. (See Figure 24)

Table 17 Calibration of SSF and ASCs for Scan Pattern simulation

Geometry Measurements	Distortion (mm)	
Rotating stripe scan pattern (or user-customized)	0.42	 <p>Extract distortion value at the location of interest from models built with third scan pattern (rotating stripe)</p>

Linear Elastic	Simulation iteration	Simulation number	direction	Distortion (mm)	Simulation settings			New settings			Error%
					SSF	ASC II	ASC I	SSF	ASC II	ASC I	
	1st		rotating	0.437841	16.44	1.00	1.00	15.88	1.00	1.00	3.5%
2nd		rotating	0.42	15.88	1.00	1.00	15.89	1.00	1.00	0.0%	

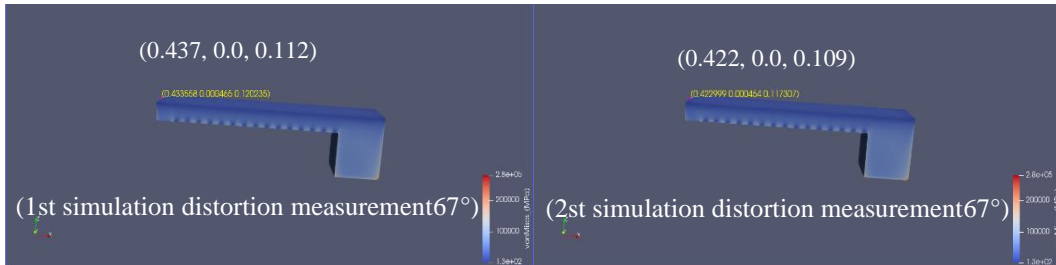
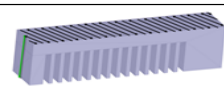


Fig. 24 Fine tuning distortion of Scan Pattern simulation

In the Thermal Strain mode, the initial simulation was kept at a certain angle (starting angle 0, rotation angle 67°) between layers without rotation using only one mode. The SSF result calibrated by the Thermal Strain simulations based on the distortion value measured from the fabricated AM sample and the distortion value measured from the shape of the simulation result is shown in Table 18.

Table 18 Calibration of SSF and ASCs for Thermal Strain simulation

Geometry Measurements	Distortion (mm)	
Rotating stripe scan pattern (or user-customized)	0.423	 <p>Extract distortion value at the location of interest from models built with third scan pattern (rotating stripe)</p>

Linear Elastic	Simulation iteration	Simulation number	direction	Distortion (mm)	Simulation settings			New settings			Error%
					SSF	ASC II	ASC I	SSF	ASC II	ASC I	
	1st		rotating	0.433558	8.5986	1.0048	0.9952	8.3892	1.0048	0.9952	2.5%
2nd		rotating	0.42	8.3892	1.0048	0.9952	8.3892	1.0048	0.9952	0.0%	

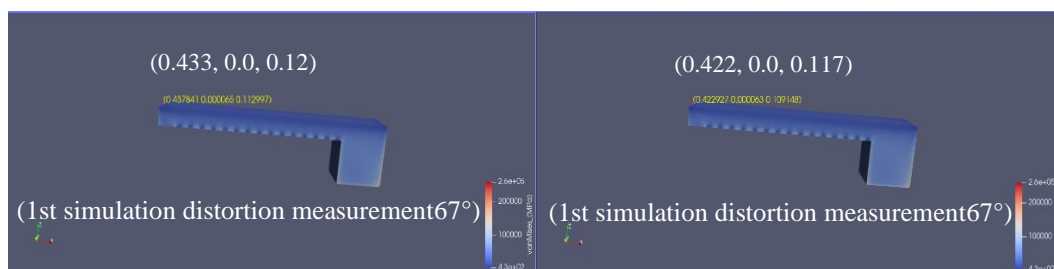


Fig. 25 Fine tuning distortion of Thermal Strain simulation

In the fine-tuning simulation of the Thermal Strain, the deformation of the first simulation resulted in a deformation error of 2.5%. This value was input for the last numerical optimization. The final SSF and ASCs values were 8.3892 and 1.0048, 0.9952. This value is closer to the actual value than the parameter simulation result adjusted in the Thermal Strain mode.

5.3 Calibration of SSF and ASCs for the measurement Point B

In the metal 3D printing process, residual stress usually has a great impact on the part when the support is removed, such as warping, deformation or even cracking. Macroscopic shape control and microscopic control have always been serious problems in the research of metal additives. Due to the removal of the support structure, the residual stress in the part can be released unrestrictedly, and the deformation of the part will have a different effect than before the support is removed. Therefore, after removing the support, a hypothetical strain model and thermal strain model simulation were performed in the Scan Pattern mode at point B.

It is to predict and optimize the SSF and ASC parameters in the AM process to increase confidence in the simulation software. The calculation of SSF and ASCs at Point B is as follows: In the Assumed Strain mode, the initial simulation was kept at a certain angle(starting angle 0, rotation angle 0) between layers without rotation using only one mode. The SSF result calibrated by Assumed Strain simulations based on the distortion value measured from the fabricated AM sample and the distortion value measured from the shape of the simulation result is shown in Table 19. The initial simulation deformation in the strain model is 0.026633, but the secondary simulation,

the deformation of point B is 0.18 mm. The deformation is large, but the error is close to zero. (See Fig. 27)

Table 19 Calibration of SSF Assumed Strain simulations

		Distortion (mm)	
Geometry Nominal			
Measurement		0.2	

Linear Elastic	Simulation iteration	Simulation number	Distortion (mm)	Simulation settings	New settings	Error%
				SSF	SSF	
	1st			0.026633	1	6.7585
2nd			0.18	6.7585	6.7585	0.0%

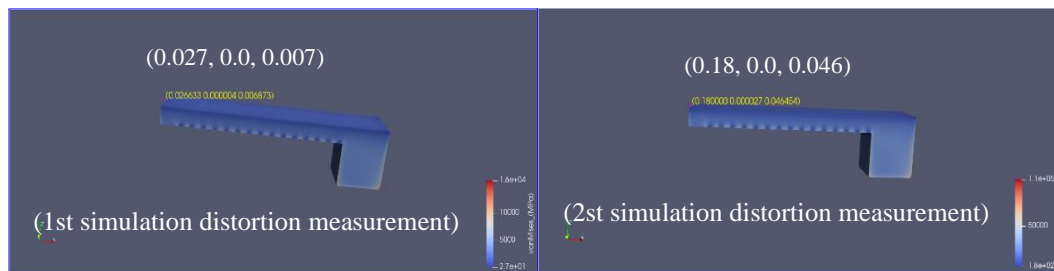


Fig. 26 Distortion of Assumed Strain simulations

In the Scanning Pattern mode, the initial simulation was kept at a certain angle(starting angle 0, rotation angle 0) and(starting angle 90, rotation angle 0) using two mode. The SSF and ASCs result calibrated by scanning simulations based on the distortion value measured from the fabricated AM sample and the distortion value measured from the shape of the simulation result is shown in Table 20. This simulation was performed two iterations using 0 degrees and 90 degrees between layers in the Scan Pattern mode. In this process, the value of SSF was optimized from 1.00 to 20.71 and 20.57, and at the same time, the value of ASC parallel to the construction direction optimized from 1.5, 0.5 to 0.33 and 1.67. The error values were optimized to 30.5% and 6.0% of 78.9% and 98.4% in the initial simulation respectively. However, in the

third simulation, the error was greatly reduced and the SSF and ASC parameters were optimized.

Table 20 Calibration of SSF and ASCs for Scan Pattern simulation

Geometry Measurements	Distortion (mm)		
direction	0.18	Extract distortion value at the location of interest from models built with scan patterns 1 and 2 (and ⊥)	
⊥ direction	0.92		

Linear Elastic	Simulation iteration	Simulation number	Distortion (mm)	Simulation settings			New settings			Error%
				SSF	ASC	ASC ⊥	SSF	ASC	ASC ⊥	
	1st		direction	0.037984	1.00	1.50	0.50	20.71	0.33	1.67
		⊥ direction	0.015128							98.4%
2nd		direction	0.236587	20.71	0.33	1.67	20.57	0.33	1.67	31.4%
		⊥ direction	0.870858							5.3%
3rd		direction	0.23	20.57	0.33	1.67	20.71	0.29	1.71	30.5%
		⊥ direction	0.86							6.0%

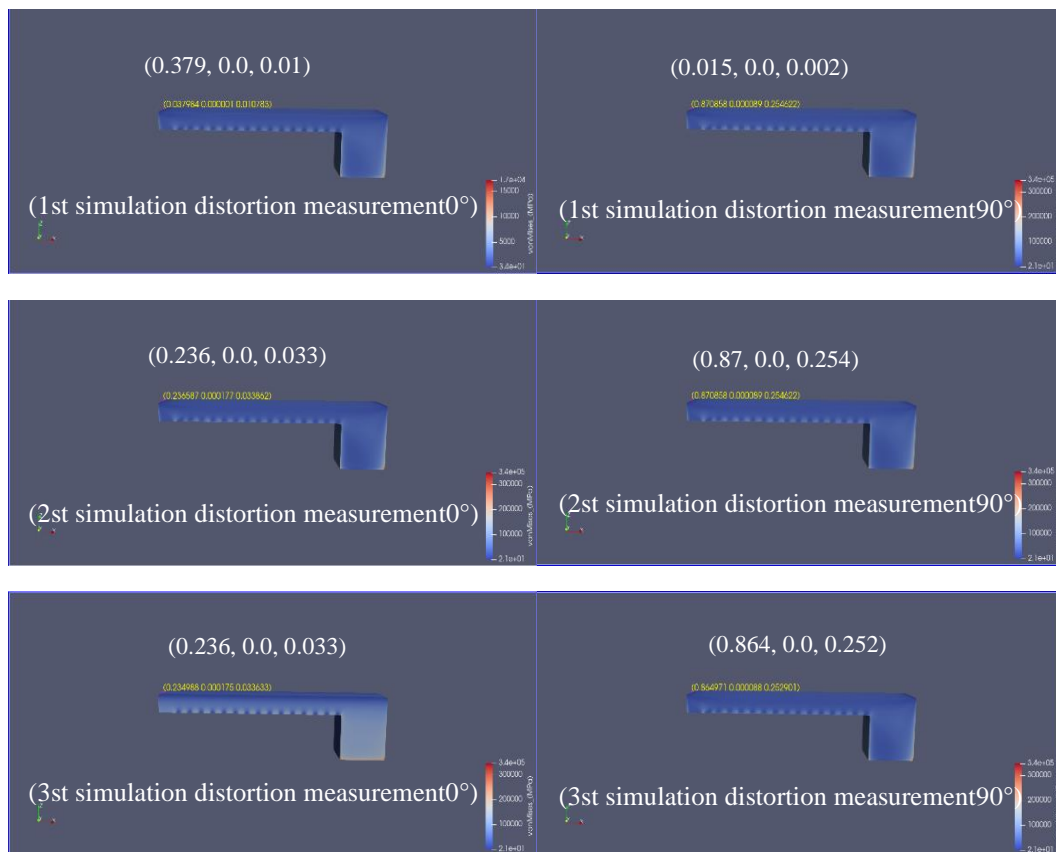
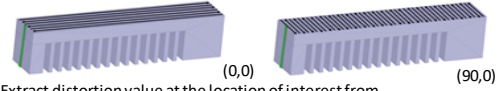


Fig. 27 Distortion of Scan Pattern simulation

In the Thermal Strain mode, the initial simulation was kept at a certain angle(starting angle 0, rotation angle 0) and(starting angle 90, rotation angle0) using

two mode. The SSF and ASCs result calibrated by the Thermal Strain simulations based on the distortion value measured from the fabricated AM sample and the distortion value measured from the shape of the simulation result is shown in Table 21. In the Thermal Strain mode, the initial SSF and ASCs values were set to 1.0, 1.5, and 0.5. Simulation analysis for the same scan angle between layers and 90° rotation between layers was performed. The error values were reduced from 59.7% and 96.9% to 25 % and 4.4%.

Table 21 Calibration of SSF and ASCs for Thermal Strain simulation

Geometry Measurements		Distortion (mm)	 Extract distortion value at the location of interest from models built with scan patterns 1 and 2 (and ⊥)	
direction		0.18		
⊥ direction		0.92		

Linear Elastic	Simulation iteration	Simulation number	Distortion (mm)	Simulation settings			New settings			Error%
				SSF	ASC	ASC ⊥	SSF	ASC	ASC ⊥	
	1st		direction	0.072601	1	1.5	0.5	10.8545	0.3273	1.6727
		⊥ direction	0.028739							96.9%
2nd		direction	0.23	10.8545	0.3273	1.6727	10.8069	0.2962	1.7038	25.0%
		⊥ direction	0.88							4.4%

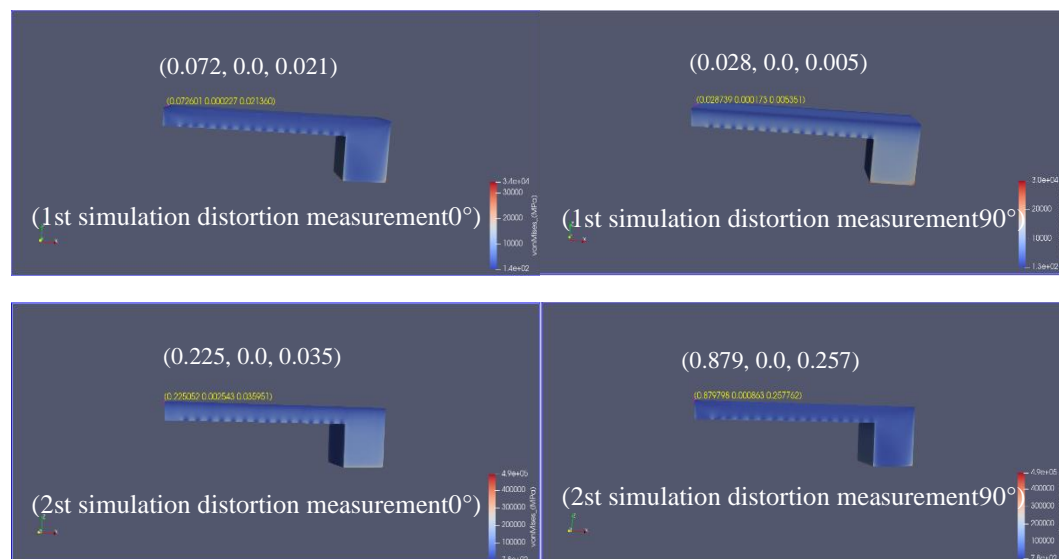


Fig. 28 Distortion of Thermal Strain simulation

5.4 Fine calibration of SSF and ASCs for the measurement Point B

The calculation of SSF and ASCs fine-tuning at Point B is as follows: In the

Assumed Strain mode, the initial simulation was kept at a certain angle (starting angle 0, rotation angle 67°) between layers without rotation using only one mode. The SSF result calibrated by Assumed Strain simulations based on the distortion value measured from the fabricated AM sample and the distortion value measured from the shape of the simulation result is shown in Table 22. In the process of using micro-control, the deformation amount of the assumed strain model with 67° rotation between layers is 0.89 mm. Compared with the 0.18 after the first optimization, a deformation amount closer to the actual value is obtained, and a reference was set.

Table 22 Calibration of SSF Assumed Strain simulations

		Distortion (mm)
Geometry Nominal		
Measurement		0.89

Linear Elastic	Simulation iteration	Simulation number	Distortion (mm)	Simulation settings	New settings	Error%
				SSF	SSF	
	1st		0.18	6.76	33.42	79.8%
2nd		0.890064	33.42	33.41	0.0%	

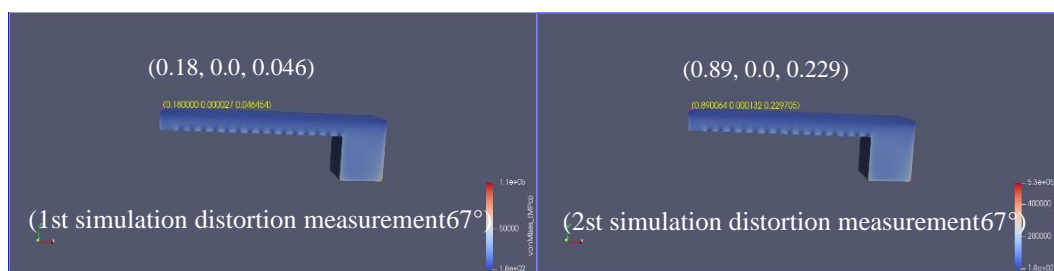
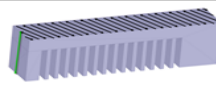


Fig. 29 Fine tuning distortion of Assumed Strain simulations

In the Scan Pattern mode, the initial simulation was kept at a certain angle (starting angle 0, rotation angle 67°) between layers without rotation using only one mode. The SSF result calibrated by the Scan Pattern simulations based on the distortion value measured from the fabricated AM sample and the distortion value measured from the

shape of the simulation result is shown in Table 23. In the fine-tuning simulation of the Scan Pattern mode, the deformation of the first simulation resulted in a deformation error of 34.6%. This value was input in simulation software for the last numerical optimization. The final SSF and ASCs values were 31.65 and 0.29, 1.71. This value is closer to the actual value than the parameter simulation result adjusted in the Assumed Strain mode.

Table 23 Calibration of SSF and ASCs for Scan Pattern simulation

Geometry Measurements		Distortion (mm)		 Extract distortion value at the location of interest from models built with third scan pattern (rotating stripe)
Rotating stripe scan pattern (or user-customized)		0.89		

	Simulation iteration	Simulation number	direction	Distortion (mm)	Simulation settings			New settings			Error%
					SSF	ASC	ASC ⊥	SSF	ASC	ASC ⊥	
	1st		rotating	0.58241	20.71	0.29	1.71	31.65	0.29	1.71	34.6%
	2nd		rotating	0.89	31.65	0.29	1.71	31.65	0.29	1.71	0.0%

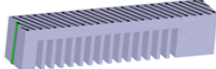


Fig. 30 Fine tuning distortion of Scan Pattern simulation

In the Thermal Strain mode, the initial simulation was kept at a certain angle(starting angle 0, rotation angle 67) between layers without rotation using only one mode. The SSF result calibrated by the Thermal Strain simulations based on the distortion value measured from the fabricated AM sample and the distortion value measured from the shape of the simulation result is shown in Table 24. In the fine-tuning simulation of the Thermal Strain, the deformation of the first simulation resulted

in a deformation error of 37.6%. This value was input in simulation software for the last numerical optimization. The final SSF and ASCs values were 17.305 and 0.2962, 1.7038, respectively. This value is closer to the actual value than the parameter simulation result adjusted in the Scan Pattern mode.

Table 24 Calibration of SSF and ASCs for Thermal Strain simulation

Geometry Measurements		Distortion (mm)	 Extract distortion value at the location of interest from models built with third scan pattern (rotating stripe)	
Rotating stripe scan pattern (or user-customized)		0.89		

Linear Elastic	Simulation iteration	Simulation number	direction	Distortion (mm)	Simulation settings			New settings			Error%
					SSF	ASC II	ASC I	SSF	ASC II	ASC I	
	1st			rotating	0.555625	10.8069	0.2962	1.7035	17.3105	0.2962	1.7038
2nd			rotating	0.89	17.3105	0.2962	1.7038	17.3105	0.2962	1.7038	0.0%

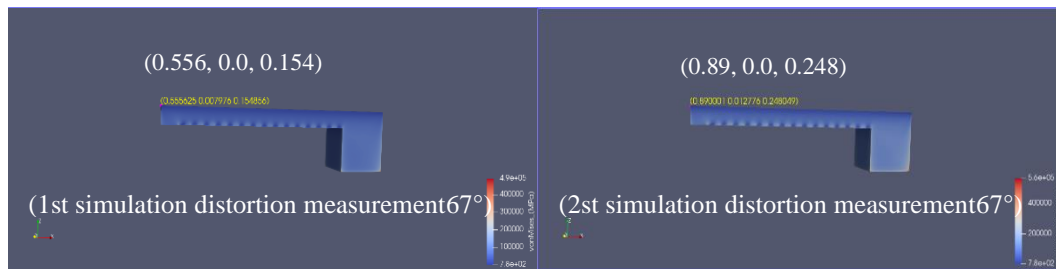


Fig. 31 Fine tuning distortion of Thermal Strain simulation

Chapter 6 Conclusion

6.1 Research results

This research aims to establish a simulation method for correcting SSF and ASC factors to improve the accuracy of the simulation software in the additive manufacturing process of maraging steel C300 powder material.

For this study, two studies were conducted to achieve the aims. First, the shape of the AM sample was analyzed through literature investigation on the existing AM simulation research. And the sample shape for AM simulation of this study was selected from the analyzed result. Second, based on the selected sample shape, the scaling factor was corrected through the manufacture and measurement of AM samples and iterative simulation.

For the sample shape analysis for AM simulation of the existing research, analysis of the sample shape applied to the simulation, analysis of the result derived from the simulation, simulation and result analysis using the existing AM sample shape, verification for generalization of AM simulation sample shape, and comparative analysis of distortion according to length in the same AM sample shape were conducted. In the analysis study of the sample shape for AM simulation, the following results were obtained.

In the existing AM simulation studies, the shape of the AM sample is mostly long and shows a simple shape structure. Most of these geometric structures represent a beam or bridge shape. It can be seen that these structures are the simplest shapes in additive manufacturing, and are easily deformed, and are easily measured for distortion.

The existing AM simulation studies mainly focus on inherent strain, residual stress

and distortion, and thermal compensation. This means that their physical properties cause the biggest problem in the additive manufacturing process of AM components. In other words, it can be solved by minimizing distortion due to residual stress in manufacturing AM components. The residual stress problem can be solved by optimizing the AM environment through AM simulation or by predicting distortion and compensating for the AM shape.

In AM simulation, the influence of the scaling factor is considered to be more affected by the length and thermal effect of the AM sample geometry than the equipment and materials used. In particular, when the height of the AM sample is high and the thickness is thin, it is highly affected by distortion. It is more affected when it is a solid type than a latex type. In addition, the distortion is largely influenced by the scan pattern, part's thickness and length, and cooling area, but it seems to have little effect on the complexity of the shape.

Based on the AM simulation shapes applied in previous studies, was analyzed as follows from the simulation results performed directly: The thinner the thickness of the AM sample shape end, the smaller the distortion in the longitudinal direction of the part. The longer the shape of the AM sample, the greater the distortion in the height direction. The larger the size of the part, the greater the distortion. The more complex the shape, the smaller the distortion. As described above, specificity was shown according to the shape of the AM sample, but no significant singularity was found about the selection criteria of the AM sample shape.

In the additive manufacturing module of ANSYS, we used three simulation modes:

assumed strain mode, thermal strain mode and scanning mode. The initial simulation of SSF and ASC factor correction was carried out by applying the assumed value, and the initial 0° and 90° . After the scanning mode of interlayer rotation, it was compared with the sample printed by additive manufacturing, and the fine simulation parameter adjustment of 67° interlayer rotation was performed. The actual deformation of the sample was measured using two methods of 3D scanning with vernier calipers.

The calibration result of the scaling factor by measuring the distortion of point A is as follows: This result is only applicable when using W Company's PBF equipment and maraging steel C300 powder material.

(1) The correction value SSF of the optimized shape in the assumed strain and scanning mode is 15.89, while in the thermal strain mode, the SSF is optimized value is 8.3892. (In the case of using W company's PBF equipment and maraging steel C300 powder material)

(2) the correction value ASC_{\parallel} and ASC_{\perp} of the optimized shape in the scanning mode is both 1, and the value of $ASC_{\parallel} = 1.0048, ASC_{\perp} = 0.9952$ in the thermal strain mode respectively.

After the deformation of point B, we obtain the optimization results of the process parameters SSF and ASCs in the three simulation modes as follows:

(1) the correction value SSF of the optimized shape in the assumed strain mode is 33.41 scan pattern mode is 31.65, while in the thermal strain mode, the SSF is optimized value is 17.3105.

(2) Using W the correction value ASC_{\parallel} and ASC_{\perp} of the optimized shape in the

scan pattern simulation is $ASC_{\parallel} = 0.29$, $ASC_{\perp} = 1.71$ and the value of $SC_{\parallel} = 0.2962$, $SC_{\perp} = 1.7038$ in the thermal strain simulation respectively.

The final validation of the scaling factor derived through this study can be confirmed through shape compensation of the AM sample and manufacturing of the AM sample. However, it was not verified in this study. Therefore, this study needs additional research in the future.

According to this AM simulation study, the effect of scaling factor for simulation software was found to be insignificant. This was found in the manufacturing and measurement process of the AM sample. As in this study, since the AM sample manufactured by the PBF method has a rough surface, it was difficult to accurately measure the distortion. And since it was a small AM sample, there was almost no distortion.

If the distortion is small as in this study, the reliability of the simulation experienced that significantly lowered due to a measurement error occurring in the process of measuring the distortion of the AM sample. In order to obtain the effect of AM simulation, it was found that it is possible when the size of the AM simulation shape becomes more than a certain level. The scaling factor obtained through AM simulation seems to be valid only when the used equipment, material, shape, size, etc. are specified. It seems difficult to generalize the scaling factor in AM simulation.

6.2 Future research topics

(1) A study is needed to compensate the shape of the AM sample using the scaling factor derived in this study and to verify it through the manufacture of the AM sample.

(2) In order to increase the accuracy of shape correction for AM sample simulation, it is necessary to study the properties of the molten pool according to materials and equipment, and the effects on the mechanism of formation of defects and mechanical properties in the thermal stress distribution process.

REFERENCE

- [1] KEICHER D M, SMUGERESKY J E, ROMERO J A, et al. Using the laser engineered net shaping (LENS) process to produce complex components from a CAD solid model[C], Proceedings of the SPIE-The International Society for Optical Engineering, Lasers as Tools for Manufacturing, Orlando, 1997
- [2] HUANG Weidong, LI Yanmin, FENG Liping, et al. Laser solid forming of metal powder materials[J]. Journal of Material Engineering, 2002(3):40-43A
- [3] MERCELISP, KRUTHJ P. Residual stresses in selective laser sintering and selective laser melting[J]. Rapid Prototyping Journal, 2006,12(5):254-265.
- [4] BASSL, MILNERJ, GNÄUPEL-HEROLDT, et al. Residual stress in additive manufactured nickel alloy 625 parts[J]. ASME: Journal of Manufacturing Science and Engineering, 2018, 140(6):061004-01-061004-11.
- [5] HODGEN E, FERENCZR M, VIGNESR M. Experimental comparison of residual stresses for a thermomechanical model for the simulation of selective laser melting[J]. Additive Manufacturing, 2016,12:159-168.A
- [6] SUÁREZA, AMADOJ M, TOBARM J, et al. Study of residual stresses generated inside laser cladded plates using FEM and diffraction of synchrotron radiation[J]. Surface and Coatings Tech-nology, 2010, 204(12/13):1983-1988.A
- [7] BROWND W, BERNARDINJ D, CARPENTERJ S, et al. Neutron diffraction measurements of residual stress in additively manufactured stainless steel[J]. Materials Science and Engineering: A, 2016, 678:291-298.A
- [8] MOATR J, PINKERTONA J, LIL, et al. Residual stresses in laser direct metal deposited waspaloym[J]. Materials Science and Engineering: A, 2011, 528(6):2288-2298.A
- [9] DINGJ, COLEGROVEP, MEHNENJ, et al. Thermo-mechanical analysis of wire and arc additive layer manufacturing process on large multi-layer parts[J]. Computational Materials Science, 2011, 50(12):3315-3322.A
- [10] MUKHERJEET, ZUBACKJ S, ZHANGW, et al. Residual stresses and distortion in additively manufactured compositionally graded and dissimilar joints[J]. Computational Materials Science, 2018, 143:325-337.
- [11] ALESSANDROS, ELEONORAA, LUCAI, et al. Experimental analysis of residual stresses on AlSi10Mg parts produced by means of selective laser melting (SLM) [J]. Procedia CIRP, 2017, 62:458-463.
- [12] BAILEYN S, KATINASC, SHINY C. Laser direct deposition of AISI H13 tool steel powder with numerical modeling of solid phase transformation, hardness, and residual stresses[J]. Journal of Materials Processing Technology, 2017, 247:223-233.
- [13] SZOSTB A, TERZIS, MARTINAF, et al. A comparative study of additive manufacturing techniques: Residual stress and microstructural analysis of CLAD and WAAM printed Ti-6Al-4V components[J]. Materials & Design, 2016, 89:559-567.

- [14] Iñaki Setien, et al, Empirical methodology to determine inherent strains in additive manufacturing, *Computers & Mathematics with Applications*,2019,78:2282-2295
- [15] X Song, S Feih, W Zhai, et al. Advances in additive manufacturing process simulation: Residual stresses and distortion predictions in complex metallic components. *Material&Design*,2020,193:108779
- [16] P Promoppatum, SC Yao, et al. Influence of scanning length and energy input on residual stress reduction in metal additive manufacturing: Numerical and experimental studies. *Journal of Manufacturing Process*,2020,49:247-259
- [17] C Li, JF Liu, YB Guo, et al. Efficient Multiscale Prediction of Cantilever Distortion by Selective Laser Melting. *Solid Freeform Fabrication 2016: Proceedings of the 27th Annual International*,2016
- [18] P Alvarez, J Ecnarro, et al. Computationally efficient distortion prediction in Powder Bed Fusion Additive Manufacturing. *International Journal of Engineering Research & Science (IJOER)*,2016,2:2395-6992
- [19] RJ Williams, CM Davies, PA Hooper, et al. Pragmatic Part Scale Model for Residual Stress and Distortion Prediction in Powder Bed Fusion. *Additive manufacture*,2018,22:416-425
- [20] C Wang, S Li, D Zeng, X Zhu, et al. An Artificial-intelligence/Statistics Solution to Quantify Material Distortion for Thermal Compensation in Additive Manufacturing,2005,09084
- [21] H Huang, J Chen, Stress and Distortion Simulation of Additive Manufacturing Process by High Performance Computing, *Pressure Vessels and Piping Conference*,2018,2018-85045
- [22] Y Zhang, J Zhang, et al. Finite Element Simulation and Experimental Validation of Distortion and Cracking Failure Phenomena in Direct Metal Laser Sintering Fabricated Component. *Additive manufacture*.2017,16:49-57
- [23] A Olleak, Z Xi, Efficient LPBF process simulation using finite element modeling with adaptive remeshing for distortions and residual stresses prediction, *Manufacturing Letters*,24:140-144
- [24] D Bompos, J Chaves, et al. Shape distortion prediction in complex 3D parts induced during the selective laser melting process. *CIRP Annals*.2020,69:517-520
- [25] H Huang, N Ma, J Chen, Toward large-scale simulation of residual stress and distortion in wire and arc additive manufacturing. *Additive manufacturing*, 2020,34:101248
- [26] S Gao, Z Tan, et al. Effects of geometrical size and structural feature on the shape-distortion behavior of hollow Ti-alloy blade fabricated by additive manufacturing process. *Journal of Laser Applications*,2020,32,032005
- [27] X Lu, X Lin, et al. Residual stress and distortion of rectangular and S-shaped Ti-6Al-4V parts by Directed Energy Deposition: Modelling and experimental calibration. *Additive manufacturing*. 2019, 26:166-179
- [28] T Mayer, G Brändle, et al. Simulation and validation of residual deformations in additive manufacturing of metal parts. *Heilyon*, 2020,6:e03987
- [29] H Huang, J Chen, et al. Stress and Distortion Simulation of Additive

- Manufacturing Process by High Performance Computing, Pressure Vessels and Piping Conference, Pvp2018-85045
- [30] P Alvarez, J Ecnarro, et al. Computationally efficient distortion prediction in Powder Bed Fusion Additive Manufacturing. International Journal of Engineering Research & Science (IJOER).
- [31] RJ Williams, CM Davies, et al. A Pragmatic Part Scale Model for Residual Stress and Distortion Prediction in Powder Bed Fusion. Additive Manufacture. 2018,22:416-425
- [32] A Inozemtsev, O Smetannikov, et al. Numerical simulation in additive manufacturing of gas turbine parts. IOP Conference Series: Materials Science and Engineering. 2020
- [33] H. K Kim and M. Yamanaka, Prediction and elimination of ductile fracture in cold forgings using FEM simulation, Engineering Research Center for Net shape Manufacturing, Columbus, 1995
- [34] Jujie Yan, Yinghao Zhou, Ruinan Gu, Xingmin Zhang, Wai-Meng Quach, and Ming Yan, "A Comprehensive Study of Steel Powders (316L, H13, P20 and 18Ni300) for Their Selective Laser Melting Additive Manufacturing," Metals 2019, 9(1), 86
- [35] T Mayer, G Brändle, et al. Simulation and validation of residual deformations in additive manufacturing of metal parts. Heliyon.2020.6:e03987
- [36] X Song, S Feih, et al. Advances in additive manufacturing process simulation: residual stresses and distortion prediction in complex metallic components. Materials & Design, 2020, 193:108779
- [37] Additive User's Guide (Print and Science), ANSYS 2020R1. P 52, P 76, <https://storage.ansys.com/mbu-assets/additive/Calibration/calibration.html>
- [38] Additive Calibration Guide, ANSYS 2020R1 P 5, P 9, P 31, <https://storage.ansys.com/mbu-assets/additive/Calibration/calibration.html>
- [39] Taesung S&E., <https://www.tsne.co.kr/pc/public/sub2/7-4-0.php>.
- [40] J. W. An et al., "Development of Analytical Model of Spindle and Rack Gear Systems for Knuckle Boom Crane", Journal of Drive and Control, Vol.14, No.2, pp.23-29, 2017.
- [41] H. G. Kim et al., "Shape Optimization for Enhancing the Performance of an Inducer for the Main Hydraulic Pump in a Rotary Wing Aircraft", Journal of Drive and Control, Vol.14, No.2, pp.37-44, 2017.